

Bioaccumulation of therapeutic drugs by human gut bacteria

<https://doi.org/10.1038/s41586-021-03891-8>

Received: 25 February 2019

Accepted: 10 August 2021

Published online: 8 September 2021

 Check for updates

Martina Klünemann^{1,9,21}, Sergej Andrejev^{1,10,21}, Sonja Blasche^{1,2,21}, Andre Mateus^{1,21}, Prasad Phapale¹, Saravanan Devendran¹, Johanna Vappiani³, Bernd Simon¹, Timothy A. Scott⁴, Eleni Kafkia², Dimitrios Konstantinidis¹, Katharina Zirngibl^{1,2}, Eleonora Mastrorilli¹, Manuel Banzhaf^{1,11}, Marie-Therese Mackmull^{1,12}, Felix Hövelmann¹, Leo Nesme^{1,13}, Ana Rita Brochado^{1,14}, Lisa Maier^{1,15}, Thomas Bock^{1,16}, Vinita Periwal^{1,2}, Manjeet Kumar¹, Yongkyu Kim¹, Melanie Tramontano^{1,10}, Carsten Schultz^{1,17}, Martin Beck^{1,18}, Janosch Hennig^{1,19}, Michael Zimmermann¹, Daniel C. Sévin³, Filipe Cabreiro^{4,5,20}, Mikhail M. Savitski¹, Peer Bork^{1,6,7,8}, Athanasios Typas¹ & Kiran R. Patil^{1,2}

Bacteria in the gut can modulate the availability and efficacy of therapeutic drugs. However, the systematic mapping of the interactions between drugs and bacteria has only started recently¹ and the main underlying mechanism proposed is the chemical transformation of drugs by microorganisms (biotransformation). Here we investigated the depletion of 15 structurally diverse drugs by 25 representative strains of gut bacteria. This revealed 70 bacteria–drug interactions, 29 of which had not to our knowledge been reported before. Over half of the new interactions can be ascribed to bioaccumulation; that is, bacteria storing the drug intracellularly without chemically modifying it, and in most cases without the growth of the bacteria being affected. As a case in point, we studied the molecular basis of bioaccumulation of the widely used antidepressant duloxetine by using click chemistry, thermal proteome profiling and metabolomics. We find that duloxetine binds to several metabolic enzymes and changes the metabolite secretion of the respective bacteria. When tested in a defined microbial community of accumulators and non-accumulators, duloxetine markedly altered the composition of the community through metabolic cross-feeding. We further validated our findings in an animal model, showing that bioaccumulating bacteria attenuate the behavioural response of *Caenorhabditis elegans* to duloxetine. Together, our results show that bioaccumulation by gut bacteria may be a common mechanism that alters drug availability and bacterial metabolism, with implications for microbiota composition, pharmacokinetics, side effects and drug responses, probably in an individual manner.

Therapeutic drugs can have a strong effect on the gut microbiome and vice versa^{2–5}. The underlying drug–bacteria interactions can reduce microbial fitness⁶ or alter drug availability through biotransformation^{7–14}. The latter can have either a positive or a negative effect on drug activity and efficacy. Although drugs such as lovastatin and sulfasalazine are chemically transformed by gut bacteria into their active forms, bacterial metabolism can inactivate drugs such as digoxin^{15,16}, or cause toxic effects as in the case of irinotecan¹⁷. Furthering the diversity of susceptible drugs, over one hundred molecules were recently reported

to be chemically modified by gut bacteria¹. Yet the mechanistic view of these interactions is largely confined to drug biotransformation^{12,13}.

Drug accumulation without metabolism

To expand our knowledge of the effects of bacteria on drug availability, we systematically profiled interactions between 15 human-targeted drugs and 25 representative strains of human gut bacteria (21 species; with additional subspecies or conspecific strains of *Bifidobacterium*

¹European Molecular Biology Laboratory, Heidelberg, Germany. ²Medical Research Council Toxicology Unit, Cambridge, UK. ³Cellzome, GlaxoSmithKline R&D, Heidelberg, Germany. ⁴Institute of Structural and Molecular Biology, University College London, London, UK. ⁵Institute of Clinical Sciences, Imperial College London, London, UK. ⁶Max Delbrück Centre for Molecular Medicine, Berlin, Germany. ⁷Yonsei Frontier Lab (YFL), Yonsei University, Seoul, South Korea. ⁸Department of Bioinformatics, Biocenter, University of Würzburg, Würzburg, Germany. ⁹Present address: Evonik Operations GmbH, Essen, Germany. ¹⁰Present address: German Cancer Research Center, Heidelberg, Germany. ¹¹Present address: School of Biosciences, University of Birmingham, Birmingham, UK. ¹²Present address: ETH Zürich, Zürich, Switzerland. ¹³Present address: Molecular Health GmbH, Heidelberg, Germany. ¹⁴Present address: University of Würzburg, Würzburg, Germany. ¹⁵Present address: University of Tübingen, Tübingen, Germany. ¹⁶Present address: Biozentrum, University of Basel, Basel, Switzerland. ¹⁷Present address: Chemical Physiology and Biochemistry Department, Oregon Health & Science University, Portland, OR, USA. ¹⁸Present address: Max Planck Institute of Biophysics, Frankfurt am Main, Germany. ¹⁹Present address: Biophysical Chemistry Department, University of Bayreuth, Bayreuth, Germany. ²⁰Present address: CECAD, University of Cologne, Köln, Germany. ²¹These authors contributed equally: Martina Klünemann, Sergej Andrejev, Sonja Blasche, Andre Mateus. [✉]e-mail: bork@embl.de; typas@embl.de; kp533@cam.ac.uk

Article

longum, *Escherichia coli* and *Bacteroides uniformis*) (Supplementary Table 1). The bacterial species were selected to cover a broad phylogenetic and metabolic diversity representative of the healthy microbiota¹⁸ (Extended Data Fig. 1a, Supplementary Table 1). On the drug side, 12 orally administered small-molecule drugs (with a molecular weight of less than 500 Da) that are amenable to quantification based on ultra-performance liquid chromatography coupled with ultraviolet detection (UPLC–UV) were selected to span diverse chemistry, indication areas and side-effect profiles (Extended Data Fig. 1b–e, Supplementary Table 2). Three additional drugs were included as controls: digoxin, with its highly specific interaction with *Escherichia coli lenta*¹⁶; and metronidazole and sulfasalazine, which are metabolized by several gut bacteria^{19–21}.

The resulting 375 bacteria–drug pairs were tested for drug depletion in two independent screens (Methods). The bacteria were grown in gut microbiome medium (GMM)²² and the initial drug concentration was set at 50 µM, which is close to the estimated colon concentration range for many drugs⁶ and allows the reliable measurement of concentration changes. For each pair, depletion of the drug from the culture supernatant was measured using UPLC–UV analysis after 48 h of anaerobic growth (Methods). Validating the assay, the control drugs metronidazole and sulfasalazine were depleted by most of the strains, and digoxin was depleted exclusively by *E. lenta*¹⁶. A false discovery rate (FDR)-corrected *P* value cut-off of 0.05 and a threshold of 30 % depletion were used for defining interactions (on the basis of the depletion of digoxin by *E. lenta* as a case with established *in vivo* relevance; Supplementary Table 3). All of the new interactions that were found in the screen were again evaluated in independent assays performed in larger-volume cultures (Extended Data Fig. 2). The interactions with statistical support in the second assay, as well as those with support from previous studies, revealed a network that spanned all of the tested strains and 66% of the tested drugs (10 of 15) (Fig. 1). Twenty-nine of these interactions (18 species and 7 drugs) have not, to our knowledge, been previously reported.

To track the fate of the depleted drugs, we measured post-growth drug concentrations in culture supernatants as well as in total culture extracts including cells (Methods). Comparison between the two revealed 17 cases in which the drug was depleted in the supernatant but could be recovered from the total culture (Supplementary Table 3). This implied an accumulation rather than a chemical transformation of the respective drugs by bacteria. This was notable as until now, biotransformation has been recognized as the main mode of drug depletion by bacteria^{1,12–14}.

As many as 17 of the 29 newly identified interactions (14 species and 4 drugs) were bioaccumulation events; that is, storage of the drug by bacteria without modifying it. The remaining 12 interactions (8 species and 5 drugs) are likely to represent biotransformation events. Two of the five drugs—levamisole and ezetimibe—have indeed been shown to be chemically modified by other gut bacteria^{1,23}. Among the bioaccumulated drugs, the antidepressant drug duloxetine and the antidiabetic drug rosiglitazone were exclusively bioaccumulated, each in a number of different species (Fig. 1). However, biodegradation and bioaccumulation interactions were not mutually exclusive. Montelukast (which is used in the treatment of asthma) and roflumilast (which is used against chronic obstructive pulmonary disease) were bioaccumulated by some bacteria and degraded by others. On the bacterial side, all strains except *Fusobacterium nucleatum* showed both types of interaction. The conspecific strains of *B. uniformis* and *E. coli* showed no overlap in their interactions, except for those with the broadly interacting control drugs sulfasalazine and metronidazole. As individuals typically harbour different strains²⁴, it is likely that the prevalence of bioaccumulation interactions is higher than reported here.

As many human-targeted drugs have been shown to affect the growth of gut bacteria⁶, we examined whether the identified bacteria–drug interactions also resulted in altered growth. Although over 30—mostly

inhibitory—drug–bacteria interactions were detected, only 3 interactions involved both modified growth and altered drug concentration (excluding the control drugs sulfasalazine and metronidazole) (Fig. 1, Supplementary Table 3). Thus, bacteria–drug and drug–bacteria interactions appear to be largely independent.

To confirm the bioaccumulation nature of the identified bacteria–drug interactions, we used two additional analytical methods—nuclear magnetic resonance (NMR) spectroscopy and liquid chromatography coupled with mass spectrometry (LC–MS) (Methods). As a case in point, we focused on duloxetine, a widely used antidepressant that was found to be bioaccumulated by eight bacterial species. NMR spectroscopy allowed us to unambiguously detect duloxetine and confirmed that the four selected strains (*Streptococcus salivarius*, *B. uniformis*, *E. coli* IAI1 and *E. coli* ED1a) depleted it from the medium without biotransforming it (Fig. 2a, b, Extended Data Figs. 3, 4). These assays were performed using cells suspended in phosphate-buffered saline (PBS) to circumvent the complexity of the GMM medium. Although only one of the two *E. coli* strains (IAI1) bioaccumulated to an appreciable extent in GMM, both strains extensively depleted duloxetine under these nutrient-deprived conditions. The LC–MS analysis in the complex GMM medium also confirmed bioaccumulation by *Clostridium saccharolyticum* and *E. coli* IAI1 at a range of concentrations between 30 and 70 µM (Fig. 2c, Extended Data Fig. 5).

Bioaccumulation affects cell metabolism

Although biotransformation can be attributed to metabolic enzymes⁷, drug bioaccumulation is mechanistically more difficult to picture. Bioaccumulation of small molecules that are not designed to target microorganisms has been observed before in other ecosystems, such as in soil or activated sludge bioreactors^{25–28}. To investigate the molecular basis of drug bioaccumulation by gut bacteria, we set out to identify protein targets of duloxetine in bioaccumulating strains. We started by constructing an alkynated, ‘clickable’, version of the molecule to use as a bait (Extended Data Fig. 6a, Methods). Fifty-five proteins, mostly metabolic enzymes, were enriched in the pull-down from *C. saccharolyticum* lysate compared to the drug-treated control (log₂-transformed fold change ≥ 2 , FDR-adjusted *P* < 0.1) (Extended Data Fig. 6b, Supplementary Table 4). Although these results strongly indicate the binding of duloxetine to specific protein targets, the use of a structurally modified version of the molecule precludes direct conclusion. We therefore also used thermal proteome profiling (TPP)^{29,30} to systematically identify proteins that undergo structural changes (stabilization or destabilization with respect to heat-induced unfolding) after exposure to unmodified duloxetine. Supporting the click-chemistry-based assays, TPP revealed several metabolic enzymes among the proteins that respond structurally to duloxetine (Supplementary Table 5). Affected pathways include amino acid metabolism, purine and pyrimidine biosynthesis, and the pentose phosphate pathway that provides precursors for nucleotide biosynthesis (Fig. 2d, Supplementary Tables 5, 6). Many of these proteins belong to the NADH–ubiquinone dehydrogenase complex, and contain a Rossmann fold that is associated with nucleotide binding (Supplementary Table 5).

The click chemistry and TPP results suggest that protein binding is a contributing factor to duloxetine bioaccumulation. This raised the question of why the two *E. coli* strains exhibited different degrees of duloxetine bioaccumulation in GMM. We compared the two *E. coli* strains in two different TPP assays in which the drug was added either to lysed or to intact cells. While the TPP in cell lysates would uncover proteins that are stabilized or destabilized owing to direct duloxetine binding, the intact cell TPP would additionally capture, under the *in vivo* conditions, the changes in the cellular response (changes in protein interactions and activity). In the intact cell assay, the bioaccumulating IAI1 strain had almost two-fold more drug-responding proteins than did the non-bioaccumulating ED1a strain (388 versus 222 proteins), and

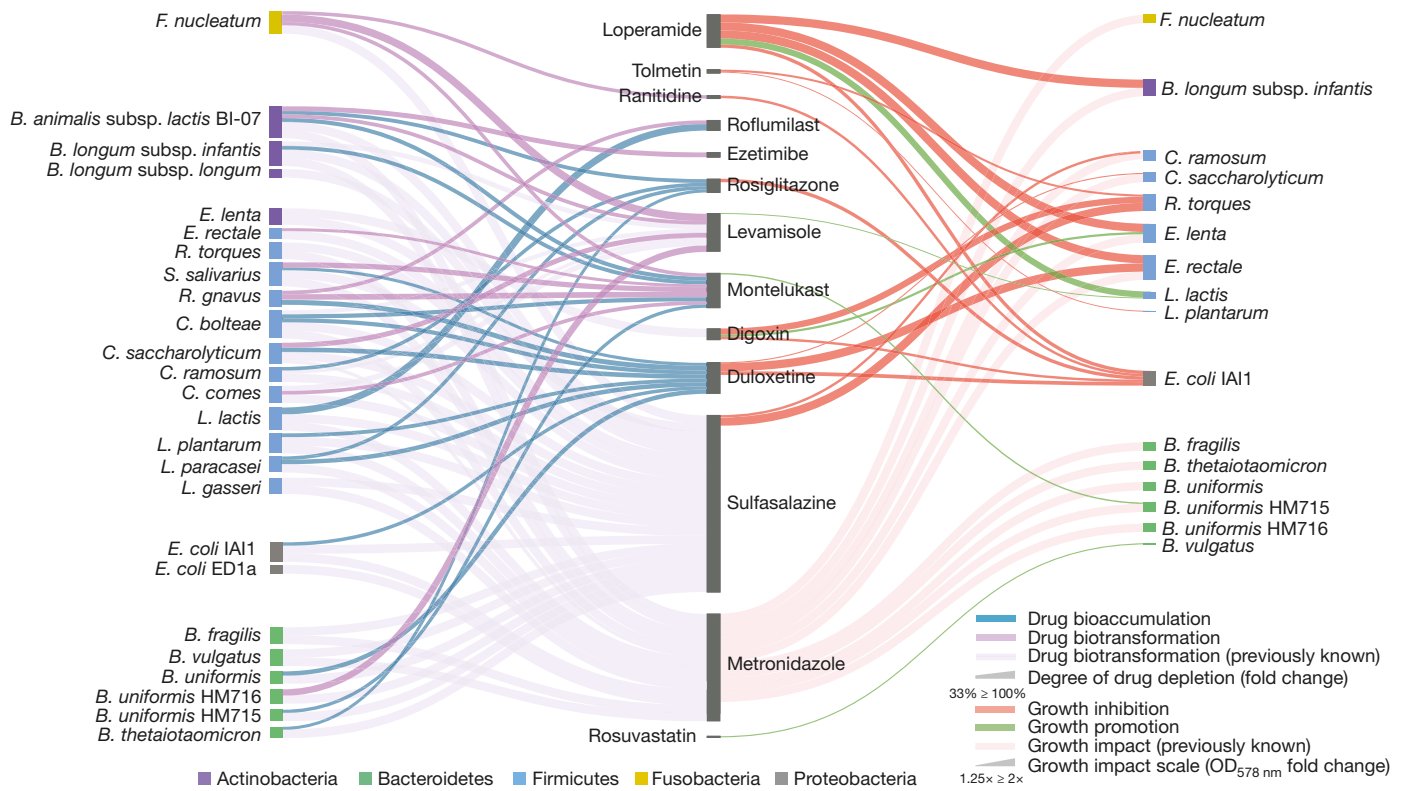


Fig. 1 | Gut bacteria accumulate therapeutic drugs without altering them.

Bacteria–drug interaction network identified in our study. Left network: biotransformation or bioaccumulation of drugs by gut bacteria. Interactions that were significant in two independent screens ($n=3$ technical replicates per screen), and validated in a follow-up assay ($n=3$ biological replicates) (Wilcoxon's rank sum test, FDR-corrected $P<0.05$) are shown. Previously reported interactions that were detected in the screen but not tested in the

validation assay are also included. Right network: the effect of drugs on the growth of gut bacteria as detected in at least two independent screens (Student's t -test, $\alpha=0.05$). $OD_{578\text{ nm}}$, optical density at 578 nm. Full names of bacteria not mentioned elsewhere in the text are as follows: *Bacteroides fragilis*, *Bacteroides vulgatus*, *Bifidobacterium animalis* subsp. *lactis* BI-07, *Coprococcus comes*, *Clostridium bolteae*, *Clostridium ramosum*, *Lactobacillus paracasei*, *Ruminococcus gnavus*.

stronger overall changes in thermal stability (Fig. 2e, Supplementary Table 5). In agreement with duloxetine changing the cellular physiology more markedly in the bioaccumulating strains, the IAI1 strain also showed a more pronounced response in differentially expressed proteins (Extended Data Fig. 6c, d, Supplementary Table 7). By contrast, the two strains exhibited very similar profiles in lysate-based TPP, in which the lack of cell envelope allows the drug to reach all intracellular proteins (397 versus 412 proteins) (Fig. 2e). It is thus likely that the strain specificity of bioaccumulation is due to differences in uptake and efflux systems, analogous to the transporter-dependent specificity observed in drug–drug interactions³¹.

The binding of duloxetine to metabolic enzymes suggests altered metabolism in bioaccumulators. To test this, we used two complementary metabolomics platforms—flow-injection analysis mass spectrometry (FIA–MS) and hydrophilic interaction chromatography coupled with tandem mass spectrometry (HILIC–MS/MS) (Methods)—to profile the effect of duloxetine treatment on small-molecule secretion by six bacterial strains (four bioaccumulating and two non-bioaccumulating). Four strains—three bioaccumulating (*C. saccharolyticum*, *Lactobacillus plantarum* and *E. coli* IAI1) and one non-bioaccumulating (*Lactococcus lactis*)—showed a significant shift in their exo-metabolome pattern after drug treatment in GMM ($P<0.05$, two-sample Hotelling's t -squared test) (Fig. 2f, Extended Data Fig. 7, Supplementary Tables 8, 9, 12A). *Clostridium saccharolyticum* was particularly notable, with the drug-induced shift in its exo-metabolome being comparable to that of interspecies differences (Fig. 2f). Furthermore, the drug response was concentration-dependent (Fig. 2g, Extended Data Fig. 7b, c), and no effect was observed for the non-bioaccumulated roflumilast (Extended

Data Fig. 8a). The concentration-dependent response to duloxetine was further validated with a subset of 71 metabolites, the chemical identity of which was putatively assigned—with two metabolites confirmed using chemical standards—using tandem mass spectrometry (Methods, Extended Data Fig. 8b, Supplementary Table 10). *Clostridium saccharolyticum* also showed a strong metabolic response to duloxetine when probed in nutrient-deprived PBS buffer (Supplementary Tables 11, 12B, Fig. 2d, Extended Data Fig. 6e–h). Together, the proteomic and metabolomic data show that duloxetine binds to abundant metabolic enzymes, supporting its intracellular storage.

Bioaccumulation induces cross-feeding

Metabolic interactions are fundamental in shaping the composition of gut microbial communities^{32,33}. We therefore asked whether metabolic changes associated with bioaccumulation can affect community composition. To address this, we assembled stable communities of five gut bacterial species (*Bacteroides thetaiotaomicron*, *Eubacterium rectale*, *Lactobacillus gasseri*, *Ruminococcus torques* and *Streptococcus salivarius*) in the presence and in the absence of duloxetine. One of the five species is a duloxetine bioaccumulator (*S. salivarius*) and another is directly inhibited by duloxetine (*E. rectale*). The five species were co-inoculated in GMM and subsequently transferred to fresh medium every 48 h. The presence of duloxetine markedly shifted the community composition, allowing *E. rectale* to increase its abundance by over 100-fold as compared to that without the drug (Fig. 3a, Extended Data Fig. 9a, b). This was notable, as *E. rectale* is the most sensitive to duloxetine among the five species that we used (Fig. 3b, Supplementary

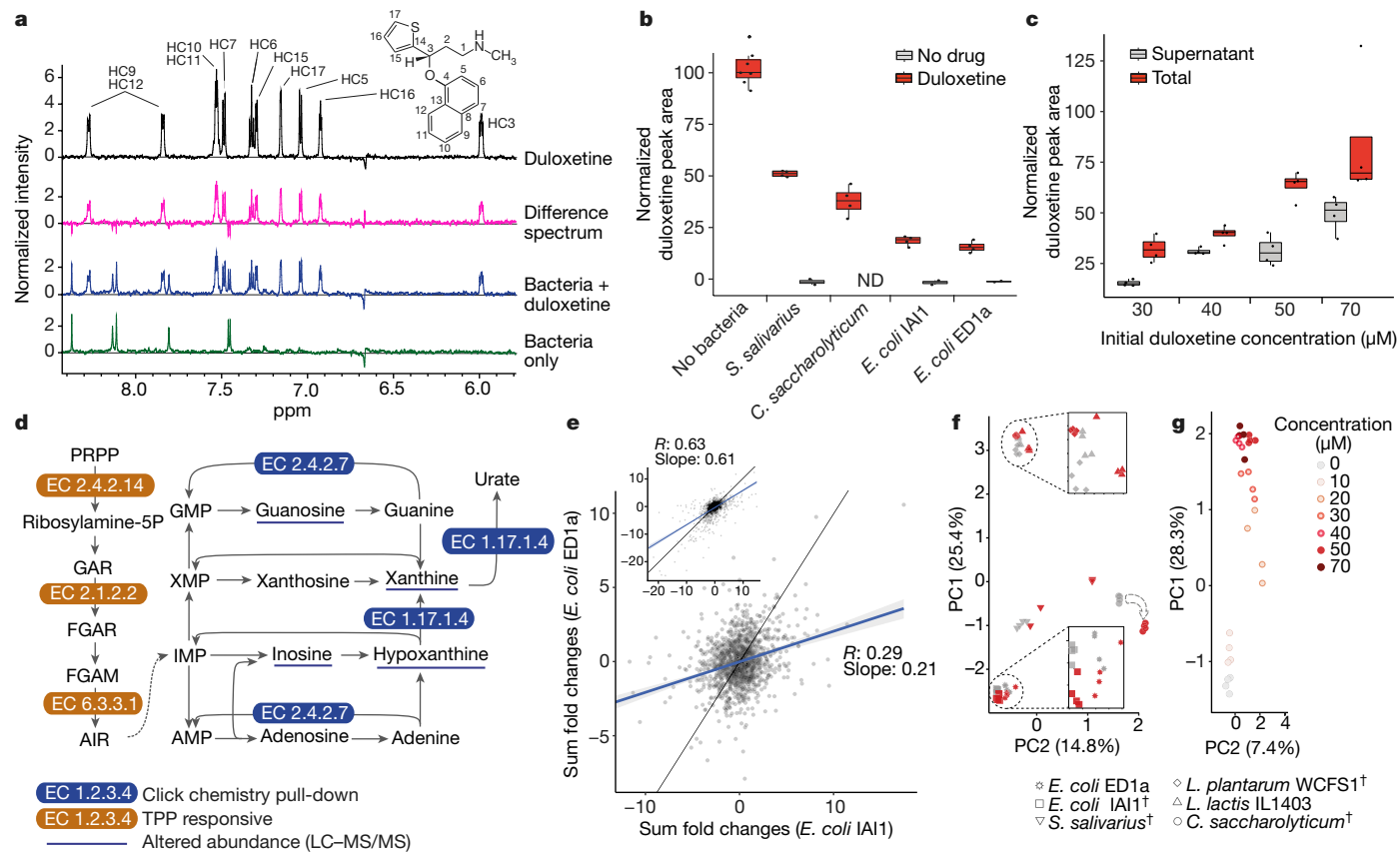


Fig. 2 | Bioaccumulation of duloxetine affects bacterial physiology. **a**, NMR analysis showing bioaccumulation of duloxetine by *S. salivarius*. Drug measurements in cell-free supernatant. The differential spectrum contrasts the drug-treated and untreated cells. **b**, NMR quantification of duloxetine in the supernatants of three gut bacterial strains treated with 50 μM duloxetine ($n = 4$ biologically independent replicates for drug treatment, $n = 2$ technical replicates for drug-free controls, $n = 7$ biologically independent replicates for bacteria-free controls). ND, no peak detected. Bioaccumulation assays in **a**, **b** performed in PBS buffer. **c**, LC-MS quantification of duloxetine in *C. saccharolyticum* bioaccumulation assays in GMM at different initial drug concentrations ($n = 4$ biologically independent replicates). Box plots in **b**, **c** show the interquartile range (IQR), the median, and whiskers extending to $1.5 \times$ IQR from the first or third quartile. **d**, *Clostridium saccharolyticum* nucleotide biosynthetic pathway marking the duloxetine-binding or -responding enzymes (Enzyme Commission (EC) numbers shown) and the differentially secreted metabolites (underlined). AMP, adenosine 5'-monophosphate; FGAM, 5'-phosphoribosyl-N-formylglycinamide; GAR, glycine amide ribonucleotide; FGAR, N-formyl-GAR; GMP, guanosine

monophosphate; IMP, inosine monophosphate; PRPP, 5-phosphoribosyl 1-pyrophosphate; XMP, xanthosine 5'-phosphate. **e**, *Escherichia coli* IAI1 (bioaccumulating in GMM) and *E. coli* ED1a (non-bioaccumulating in GMM) strains respond differently to duloxetine in TPP analysis. Each dot represents the summed log₂-transformed fold changes across all temperatures for an identified protein. Main panel, duloxetine added to intact cells before TPP (1,437 proteins in total); inset, TPP results when drug added to the cell lysates (1,694 proteins in total). Black line, diagonal; blue line, linear regression fit; error bands around the blue lines, 95% confidence interval. Data for both intact cells and lysate TPP are based on $n = 5$ independent experiments for each strain (four different drug concentrations and a vehicle control). **f**, Effect of duloxetine treatment on the exo-metabolome (untargeted HILIC-MS; Methods) of six gut bacterial strains. The numbers in parentheses mark the explained variance for the corresponding principal components (PC1 and PC2). The dotted arrow marks the duloxetine-induced shift in the exo-metabolome of *C. saccharolyticum*. The dagger symbols indicate bioaccumulating strains (GMM). **g**, Duloxetine-induced changes in the *C. saccharolyticum* exo-metabolome are concentration-dependent.

Table 13). Consistent with *S. salivarius* being a bioaccumulator, duloxetine was depleted in the community supernatant (decrease of around 15%; relative abundance of *S. salivarius* around 20%) (Extended Data Fig. 9c). Although decreased duloxetine concentration could protect *E. rectale* in the community, its bloom in the presence of duloxetine would require growth-promoting interactions.

We hypothesized that the changed metabolite secretion by *S. salivarius* in response to duloxetine could boost *E. rectale*. Supporting this, the spent medium from *S. salivarius* grown in the presence of the drug improved the growth of *E. rectale* (Fig. 3c). Untargeted metabolomics data from both FIA-MS and HILIC-MS/MS further supported the cross-feeding hypothesis. Accordingly, several metabolites were found to be accumulated during the cultivation of *S. salivarius* and subsequently depleted during *E. rectale* growth (Fig. 3d, Extended Data Fig. 9d, Supplementary Tables 14, 15). Five

of these metabolites were putatively annotated, and two—linolenic acid and glycocholic acid—were confirmed using analytical standards (Methods). The changes in nucleotide-related metabolites, such as uridine 5'-diphosphate, are in line with the proteins and metabolites affected by duloxetine (Fig. 2d), and with the fastidious nature of *E. rectale*¹⁸. Thus, human-targeted drugs can modulate gut microbial communities, not only through direct inhibition^{2,6}, but also by creating cross-feeding opportunities.

Bioaccumulation affects host response

We next investigated the effect of duloxetine bioaccumulation on host response using *C. elegans* as a model system. Duloxetine, as a serotonin–norepinephrine reuptake inhibitor, regulates the behaviour (muscular movement) of *C. elegans* in a concentration-dependent manner

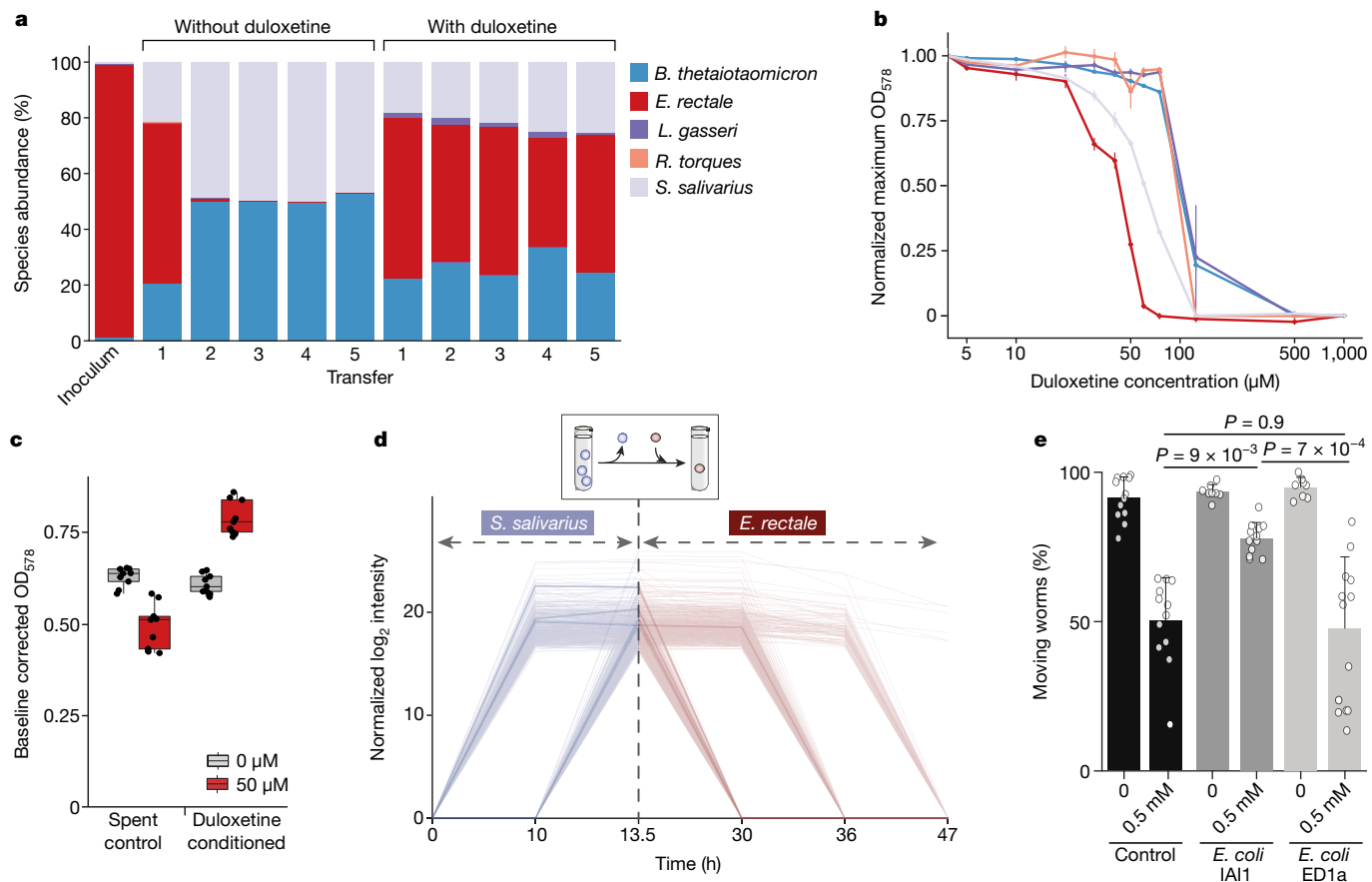


Fig. 3 | Duloxetine bioaccumulation alters community assembly and host response. **a**, Community assembly is affected by duloxetine. A starting mixture of five bacteria was transferred to fresh medium with or without duloxetine every 48 h (Methods). The profile of mean relative abundances estimated using 16S rRNA amplicon sequencing is shown (biological triplicates). Apparent initial uneven distribution is due to interspecies differences in cell lysis and gene amplification efficiency. The trend of *E. rectale* is normalized to the inoculum signal in Extended Data Fig. 9b. **b**, Mono-culture duloxetine sensitivity of the five species used in **a**. For each concentration-strain combination, $n=3$ independent growth curves. Error bars show s.d.; central circles mark the mean. **c**, $OD_{578\text{nm}}$ of *E. rectale* grown on spent medium of *S. salivarius*. The medium was supplemented with duloxetine either before (drug conditioned) or after (spent control) *S. salivarius* growth ($n=9$, three biological and three technical replicates). Box plot parameters are as in Fig. 2.

d, Metabolite profiles (956 in total; untargeted HILIC-MS analysis; Methods) that increased during the growth of *S. salivarius* in GMM and decreased during the growth of *E. rectale* in the cell-free conditioned medium of *S. salivarius*, implying cross-feeding. Thicker lines mark five metabolites putatively assigned using HILIC-MS/MS, two of which (linolenic acid and glycocholic acid) were confirmed against analytical standards. Mean intensities from three biological replicates are shown. **e**, Percentage of worms displaying movement in spent LB medium pre-incubated with 0.5 mM duloxetine in the absence or presence of *E. coli* IAI1 (bioaccumulating) or *E. coli* ED1a (non-bioaccumulating) ($n=8$ (columns 3 and 5); 4 biological \times 2 technical replicates) or 12 (all other columns; 6 biological \times 2 technical replicates). Bar heights mark the mean; error bars show s.d. P values estimated using one-way ANOVA followed by correction for multiple pairwise comparisons (Tukey's test). Duloxetine measurements are in Extended Data Fig. 9f.

(Extended Data Fig. 9e). We examined animal movement as a behavioural readout in the presence of a bioaccumulating species (*E. coli* IAI1) as part of the *C. elegans* growth medium. As a closely related control, we used the strain *E. coli* ED1a that did not bioaccumulate in complex growth medium. Indeed, only the duloxetine-bioaccumulating strain IAI1 attenuated the effect of duloxetine on the host (Fig. 3e, Extended Data Fig. 9f). Although the *C. elegans* gut is colonized by facultative anaerobes and obligate aerobes and is thus likely to be aerobic³⁴, our results agree well with the bioaccumulation observed in the anaerobic culture experiments. Further investigation of the microbiome-duloxetine-host interaction in other model systems or in a clinical setting is thus warranted.

Discussion

Our results uncover two ways in which the therapeutic effects of host-targeted drugs could be modulated owing to bioaccumulation by gut bacteria: a primary effect through reduced drug availability,

and a secondary effect through changed metabolite secretion. The latter can lead to changes in community composition, which is associated with side-effects or even the mode of action of some drugs^{2,35,36}. For our case-in-point drug duloxetine, gut bacterial interactions are indeed implicated in side effects like weight gain, and also in its mode of action^{37–39}. More broadly, our study calls for a systematic mapping of reciprocal interactions between drugs and gut bacteria—drugs that affect microorganisms and microorganisms that biotransform or bioaccumulate drugs—both individually for measuring direct effects, and in communities for estimating secondary effects.

Online content

Any methods, additional references, Nature Research reporting summaries, source data, extended data, supplementary information, acknowledgements, peer review information; details of author contributions and competing interests; and statements of data and code availability are available at <https://doi.org/10.1038/s41586-021-03891-8>.

1. Zimmermann, M., Zimmermann-Kogadeeva, M., Wegmann, R. & Goodman, A. L. Mapping human microbiome drug metabolism by gut bacteria and their genes. *Nature* **570**, 462–467 (2019).
2. Forslund, K., Hildebrand, F., Nielsen, T. & Falony, G. A. Disentangling type 2 diabetes and metformin treatment signatures in the human gut microbiota. *Nature* **528**, 262–266 (2015).
3. Falony, G. et al. Population-level analysis of gut microbiome variation. *Science* **352**, 560–564 (2016).
4. Maier, L. & Typas, A. Systematically investigating the impact of medication on the gut microbiome. *Curr. Opin. Microbiol.* **39**, 128–135 (2017).
5. Jackson, M. A. et al. Gut microbiota associations with common diseases and prescription medications in a population-based cohort. *Nat. Commun.* **9**, 2655 (2018).
6. Maier, L. et al. Extensive impact of non-antibiotic drugs on human gut bacteria. *Nature* **555**, 623–628 (2018).
7. Spanogiannopoulos, P., Bess, E. N., Carmody, R. N. & Turnbaugh, P. J. The microbial pharmacists within us: a metagenomic view of xenobiotic metabolism. *Nat. Rev. Microbiol.* **14**, 273–287 (2016).
8. Alexander, J. L. et al. Gut microbiota modulation of chemotherapy efficacy and toxicity. *Nat. Rev. Gastroenterol. Hepatol.* **14**, 356–365 (2017).
9. Fuller, A. T. Is p-aminobenzenesulphonamide the active agent in prontosil therapy? *Lancet* **229**, 194–198 (1937).
10. Goldman, P., Peppercorn, M. A. & Goldin, B. R. Metabolism of drugs by microorganisms in the intestine. *Am. J. Clin. Nutr.* **27**, 1348–1355 (1974).
11. Chhabra, R. S. Intestinal absorption and metabolism of xenobiotics. *Environ. Health Perspect.* **33**, 61–69 (1979).
12. Koppel, N., Maini Rekdal, V. & Balskus, E. P. Chemical transformation of xenobiotics by the human gut microbiota. *Science* **356**, eaag2770 (2017).
13. Sousa, T. et al. The gastrointestinal microbiota as a site for the biotransformation of drugs. *Int. J. Pharm.* **363**, 1–25 (2008).
14. Klaassen, C. D. & Cui, J. Y. Review: mechanisms of how the intestinal microbiota alters the effects of drugs and bile acids. *Drug Metab. Dispos.* **43**, 1505–1521 (2015).
15. Haiser, H. J., Seim, K. L., Balskus, E. P. & Turnbaugh, P. J. Mechanistic insight into digoxin inactivation by *Eggerthella lenta* augments our understanding of its pharmacokinetics. *Gut Microbes* **5**, 233–238 (2014).
16. Koppel, N., Bisanz, J. E., Pandelia, M.-E., Turnbaugh, P. J. & Balskus, E. P. Discovery and characterization of a prevalent human gut bacterial enzyme sufficient for the inactivation of a family of plant toxins. *eLife* **7**, e33953 (2018).
17. Wallace, B. D., Wang, H., Lane, K. T. & Scott, J. E. Alleviating cancer drug toxicity by inhibiting a bacterial enzyme. *Science* **330**, 831–835 (2010).
18. Tramontano, M. et al. Nutritional preferences of human gut bacteria reveal their metabolic idiosyncrasies. *Nat. Microbiol.* **3**, 514–522 (2018).
19. Chrystal, E. J. T., Koch, R. L., McLafferty, M. A. & Goldman, P. Relationship between metronidazole metabolism and bactericidal activity. *Antimicrob. Agents Chemother.* **18**, 566–573 (1980).
20. Mahmood, S., Khalid, A., Arshad, M., Mahmood, T. & Crowley, D. E. Detoxification of azo dyes by bacterial oxidoreductase enzymes. *Crit. Rev. Biotechnol.* **36**, 639–651 (2016).
21. Khan, A. K. A., Guthrie, G., Johnston, H. H., Truelove, S. C. & Williamson, D. H. Tissue and bacterial splitting of sulphasalazine. *Clin. Sci.* **64**, 349–354 (1983).
22. Goodman, A. L. et al. Extensive personal human gut microbiota culture collections characterized and manipulated in gnotobiotic mice. *Proc. Natl. Acad. Sci. USA* **108**, 6252–6257 (2011).
23. Shu, Y. Z. & Kingston, D. G. A. Metabolism of levamisole, an anti-colon cancer drug, by human intestinal bacteria. *Xenobiotica* **21**, 737–750 (1991).
24. Schloissnig, S. et al. Genomic variation landscape of the human gut microbiome. *Nature* **493**, 45–50 (2013).
25. Fenner, K., Canonica, S., Wackett, L. P. & Elsner, M. Evaluating pesticide degradation in the environment: blind spots and emerging opportunities. *Science* **341**, 752–758 (2013).
26. Gulde, R., Anliker, S., Kohler, H. E. & Fenner, K. Ion trapping of amines in protozoa: a novel removal mechanism for micropollutants in activated sludge. *Environ. Sci. Technol.* **52**, 52–60 (2018).
27. Congeevaram, S., Dhanarani, S., Park, J., Dexilin, M. & Thamaraiselvi, K. Biosorption of chromium and nickel by heavy metal resistant fungal and bacterial isolates. *J. Hazard. Mater.* **146**, 270–277 (2007).
28. Bae, W., Chen, W., Mulchandani, A. & Mehra, R. K. Enhanced bioaccumulation of heavy metals by bacterial cells displaying synthetic phytochelatins. *Biotechnol. Bioeng.* **70**, 518–524 (2000).
29. Becher, I. et al. Thermal profiling reveals phenylalanine hydroxylase as an off-target of panobinostat. *Nat. Chem. Biol.* **12**, 908–910 (2016).
30. Franken, H. et al. Thermal proteome profiling for unbiased identification of direct and indirect drug targets using multiplexed quantitative mass spectrometry. *Nat. Protoc.* **10**, 1567–1593 (2015).
31. Brochado, A. R. et al. Species-specific activity of antibacterial drug combinations. *Nature* **559**, 259–263 (2018).
32. Rakoff-Nahoum, S., Coyne, M. J. & Comstock, L. E. An ecological network of polysaccharide utilization among human intestinal symbionts. *Curr. Biol.* **24**, 40–49 (2014).
33. Hooper, L. V., Littman, D. R. & Macpherson, A. J. Interactions between the microbiota and the immune system. *Science* **336**, 1268–1273 (2012).
34. Zhang, F. et al. *Caenorhabditis elegans* as a model for microbiome research. *Front. Microbiol.* **8**, 485 (2017).
35. Vetizou, M. et al. Anticancer immunotherapy by CTLA-4 blockade relies on the gut microbiota. *Science* **350**, 107–107 (2015).
36. Wu, H. et al. Metformin alters the gut microbiome of individuals with treatment-naïve type 2 diabetes, contributing to the therapeutic effects of the drug. *Nat. Med.* **23**, 850–858 (2017).
37. Macedo, D. et al. Antidepressants, antimicrobials or both? Gut microbiota dysbiosis in depression and possible implications of the antimicrobial effects of antidepressant drugs for antidepressant effectiveness. *J. Affect. Disord.* **208**, 22–32 (2017).
38. Sharon, G., Sampson, T. R., Geschwind, D. H. & Mazmanian, S. K. The central nervous system and the gut microbiome. *Cell* **167**, 915–932 (2016).
39. Dent, R. et al. Changes in body weight and psychotropic drugs: a systematic synthesis of the literature. *PLoS ONE* **7**, e36889 (2012).

Publisher's note Springer Nature remains neutral with regard to jurisdictional claims in published maps and institutional affiliations.

© The Author(s), under exclusive licence to Springer Nature Limited 2021

Methods

Data reporting

No statistical methods were used to predetermine sample size. The experiments were not randomized and the investigators were not blinded to allocation during experiments and outcome assessment.

Growth conditions

Unless otherwise indicated, all bacteria were grown as liquid cultures in GMM²². Culturing was carried out in a vinyl anaerobic chamber (COY) at 37 °C with oxygen below 20 ppm, 15% carbon dioxide and 1.8–2% hydrogen. The main gas in the anaerobic chamber was nitrogen. All experimental cultures were started from the second passage culture after inoculation from a glycerol or DMSO stock. All media, buffer, glass and plasticware used in the study were exposed to the anaerobic conditions at least 12 h before use.

Bacteria–drug interaction screen

For all drugs, a fixed concentration of 50 µM was used, which is within the colon concentration range estimated for many drugs⁶. Triplicates for each bacterium–drug interaction and a single bacteria-free control were screened per plate and drug. Bacteria-free controls from multiple plates within a batch were pooled together (at least 4 per drug, median of 17) for comparison with the corresponding treated samples. Wilcoxon's rank sum test and a *P* value cut-off 0.05 (after FDR correction) were used to assess statistical significance. The screen was carried out under anaerobic conditions in 96-well plates (Nunclon Delta Surface 163320, NUNC) with 150 µl GMM as the growth medium sealed with a Breathe-Easy sealing membrane (Z380059, Sigma-Aldrich). Plates containing 100 µl of the medium and 75 µM of the drug were prepared beforehand, stored at –20 °C and used as needed. Frozen plates were introduced into the anaerobic chamber the evening before inoculation. Wells were inoculated with 50 µl of a second passage culture to reach a starting OD_{578 nm} of 0.01. Growth was monitored by measuring OD_{578 nm} using an Eon Microplate Spectrophotometer (BioTek) approximately every 2 h for the first 10 h, and then approximately every 6 h. After 48 h, plates were removed from the anaerobic chamber and the bacteria were spun down (4,000 rpm, 10 min) to collect the supernatant. One hundred microlitres of it was extracted in 300 µl ice cold acetonitrile:methanol (Biosolve, ULC/MS grade) in 500 µl polypropylene plates (Corning Costar 3957) to remove compounds interfering with liquid chromatography. Plates were closed with a lid (Corning, storage mat 3080) and after shaking and 15 min incubation at 4 °C, samples were centrifuged at 4,000 rpm for 10 min at 4 °C and 300 µl of the supernatant was transferred to a new plate (Corning Costar 3362). All liquid handling outside of the anaerobic chamber was done using a ducted liquid handling robot (FXp, Biomek). Sample plates were then left overnight in a chemical hood to evaporate the organic phase, before being stored at –20 °C. For estimating the drug concentration in the samples with the UPLC, samples were reconstituted in 50 µl 20% acetonitrile solution containing 250 µM caffeine (Sigma) as an internal standard.

Screen validation and bioaccumulation detection

Bacteria from second passage culture were inoculated at a starting OD_{578 nm} of 0.01 in 1 ml GMM containing 50 µM drug of interest in 2 ml Eppendorf tubes and incubated for 48 h while shaking. After the growth, the cultures were removed from the anaerobic chamber, and 800 µl of each sample was transferred to a new Eppendorf tube, while the remaining 200 µl was directly extracted by adding 600 µl ice-cold acetonitrile:methanol solution and incubated for 15 min at 4 °C. For supernatant extraction, the transferred culture was centrifuged for 5 min at 14,000 rpm to pellet the bacteria, and 200 µl of the bacteria-free supernatant was extracted in a new Eppendorf tube, respectively. After the 15-min 4 °C incubation period, all samples were centrifuged for 10 min, 14,000 rpm at 4 °C and 700 µl of the supernatant

was transferred to a new Eppendorf tube. Samples were dried for 5–7 h at 30 °C in a speedvac (Eppendorf Vacuum Concentrator Plus, V-AL mode) and stored at –20 °C until used for UPLC measurement. Samples were reconstituted in 116 µl 20% acetonitrile containing 250 µM caffeine. All interactions and controls were tested in triplicate.

UPLC analysis

Liquid chromatography analyses were run on a Waters Acuity UPLC H-Class instrument with a PDA detector and a quaternary solvent system. Each run was around 5 min long, with a flow rate of 0.5 ml min^{–1} and run on a CSH C18 column (Waters, Part number 186005297; 130 Å, 1.7 µm, 2.1 mm × 100 mm) in reverse mode. The column was heated to 40 °C and samples were kept at 6 °C. All methods used 50% acetonitrile (Biosolve, ULC grade) as washing buffer, and 50% methanol (Biosolve, ULC grade) as purging buffer. As organic mobile phase, acetonitrile was used. The assay used two additional buffers besides water as hydrophilic mobile phase: 5 mM formic acid (Biosolve, ULC grade) of pH 3.2 and 5 mM ammonium formate (ammonium hydroxide, ACS grade, Sigma) with pH adjusted to 8.3 using formic acid. Supplementary Table 16 lists the five different chromatographic methods established for the different drugs. During the method development, we checked for the absence of interference from bacterial or growth medium metabolites by running bacteria-only and medium samples. Carrier treated bacterial cultures were also included in the screen and the corresponding UPLC results were inspected for the absence of any peaks that could overlap with the drug peak (Supplementary Fig. 1).

NMR analysis

Bacteria were grown in GMM for one or two days (depending on the growth rate of the strain) at 37 °C without shaking in an anaerobic chamber. The cells were collected by centrifugation and washed twice with PBS, pH 6.5 buffer under anaerobic conditions and then resuspended at a final optical density of 3.75 in PBS containing duloxetine or an equivalent amount of DMSO (standard DMSO or deuterated DMSO) before incubation for 4 h at 37 °C in an anaerobic chamber. Samples were then centrifuged for 2 min at 8,000 rpm to separate cells and supernatant. The supernatant was directly used for NMR analysis (540 µl). For extracting the drug from cell pellets, the pellet was resuspended in 200 µl methanol, before addition of 600 µl deuterated DMSO and 0.4 g acid-washed glass beads. Bead beating was done for 1 min at 4 °C at 6.5 m s^{–1}. For NMR analysis, 540 µl of extract without beads was used. The duloxetine concentration was quantified by comparing the peak integrals of isolated peaks to the signals of a reference spectrum of pure duloxetine dissolved in the corresponding deuterated solvent and the chemical shifts were referenced to the residual proton signal of the solvent in this spectrum. One-dimensional proton NMR spectra with water pre-saturation were measured for all samples at 298 K on a Bruker Avance III 700 MHz spectrometer equipped with a triple-resonance room temperature probe head. Each spectrum was acquired with 128 scans, using an interscan delay of 6.2 s (2.2 s acquisition time) and was processed with Topspin 3.5 (Bruker).

LC–MS/MS duloxetine measurements (reverse phase LC–MS/MS, Orbitrap)

LC–MS/MS analysis was performed on a Vanquish UPLC system coupled with Q-Exactive plus HRMS (Thermo Fisher Scientific). The injection volume was 2 µl and the separation was carried out on a Waters ACQUITY UPLC HSS T3 column (2.1 × 100 mm, 1.8 µm; Waters) at the flow rate of 0.3 ml min^{–1} and maintained at 40 °C. The mobile phase consisted of solvent A (0.1% formic acid in water) and solvent B (0.1% formic acid in methanol) with a 10-min gradient, starting at 10% of solvent B for 2 min, which was ramped up to 90% for the next 2 min and then held for 2 min followed by 4 min of equilibration to the starting condition (10% of solvent B). The analytes were detected with HRMS full scan at the mass-resolving power *R* = 35,000 in a mass range of

Article

60–900 m/z. For identification of analytes; the data-dependent tandem (MS/MS) scans were obtained along with full scans using higher-energy collisional dissociation (HCD) with normalized collision energies of 30, 35 and 40 units (at $R = 17,500$), which were then compared with MS/MS spectra obtained from authentic standards. The MS parameters in the Tune software (Thermo Fisher Scientific) were set as: ESI positive voltage of 4 kV, sheath gas 30 and auxiliary gas 5 units, S-Lens 65 eV, capillary temperature 320 °C and vaporization temperature of auxiliary gas was 250 °C. The data analysis and quantification of drugs was performed using the Xcalibur Quan Browser software (Thermo Fisher Scientific). Three internal standards were used: fluoxetine, sulfamethizole and sulfamethazine. In addition, to account for the complex matrix effects, drug standards were prepared by adding the drug to the *C. saccharolyticum* supernatants or cell lysates and extracting from these in acetonitrile:methanol in the same manner as for the samples. Solvent blanks (acetonitrile:methanol) and medium-only controls (incubated as the samples) were run intermittently to ensure that there was no drug carry-over from the system.

Click-chemistry-based identification of duloxetine-binding proteins

Bacterial suspensions of *C. saccharolyticum* (1 ml, anaerobic conditions) were lysed by bead disruption and additional sonication at 4 °C (two times at 75% amplitude, 0.5-s cycle for one minute, Hielscher sonicator). The supernatant after centrifugation at 20,000g at 4 °C for 10 min, containing protein lysate, was recovered and protease inhibitors (aprotinin 10 µg ml⁻¹, leupeptin 5 µg ml⁻¹) were added. For all duloxetine–protein pull-downs, Strep-Tactin Sepharose 50% suspension (2-1201-025, IBA) was used. For each sample, 400 µl Strep-Tactin Sepharose (50% suspension) was pre-washed three times using 400 µl PBS (pH = 7) at room temperature. Beads were bound to duloxetine before addition of the protein lysate by resuspension in 400 µl PBS containing 50 µM duloxetine (control) or 50 µM duloxetine linked to desthiobiotin (for pull-down) on a rotating wheel at room temperature for 30 min. Unbound drug was removed by three PBS wash cycles (400 µl each). Protein lysates were incubated with drug-bound beads on a rotating wheel at 4 °C overnight. Unbound proteins were removed by washing the beads with cold PBS. Bound proteins were recovered by competitive elution using PBS containing 5 mM biotin. After an SDS gel using stain-free SDS–PAGE imaging technology (Bio-Rad) showed protein integrity, samples were further processed for mass-spectrometry-based protein identification. The pull-down was conducted in quadruplicates for each treated and control sample.

For the identification of recovered proteins by mass spectrometry, protein eluates were rebuffered into 4 M urea/0.2% rapigest (final concentration) and sonicated in a vial tweeter (Hielscher) for two times 30 s (100%, 0.5-sec cycle). Disulfide bridges between cysteines were disrupted by reduction with 10 mM DTT at 37 °C for 30 min. After that, free cysteines were alkylated using 15 mM iodoacetamide at room temperature in the dark for 30 min. Protein digestion was performed using 1:100 (w/w) Lys-C endoproteinase (Wako Chemicals) at 37 °C for 4 h and then finalized (after the urea concentration was diluted to 1.6 M) with 1:50 (w/w) trypsin (Promega) at 37 °C overnight. Rapigest was cleaved by acidification below pH = 3 using 10% (v/v) TFA at room temperature for 30 min and removed by desalting of the peptide mixture using C18 spin columns (Harvard Apparatus) according to the manufacturer's procedures. Desalted peptides were vacuum-dried and stored at -20 °C until further use. These samples were analysed using a nanoAcuity UPLC system (Waters) connected online to a LTQ-Orbitrap Velos Pro instrument (Thermo Fisher Scientific). Peptides were separated on a BEH300 C18 (75 µm × 250 mm, 1.7 µm) nanoAcuity UPLC column (Waters) using a stepwise 90-min gradient between 3 and 85% (v/v) ACN in 0.1% (v/v) formic acid. Data acquisition was performed by collision-induced dissociation using a TOP-20 strategy with standard parameters. For the quantitative label-free analysis, raw files from the Orbitrap were

analysed using MaxQuant (v.1.5.3.28)⁴⁰. MS/MS spectra were searched against the *C. saccharolyticum* (strain ATCC 35040/DSM 2544/NRCC 2533/WM1) entries of the Uniprot KB (database release 2016_04, 7212 entries) using the Andromeda search engine⁴¹. The search criteria were set as follows: full tryptic specificity was required (cleavage after lysine or arginine residues, unless followed by proline); two missed cleavages were allowed; carbamidomethylation (C) was set as fixed modification; oxidation (M) and acetylation (protein N-term) were applied as variable modifications, if applicable; mass tolerance of 20 ppm (precursor) and 0.5 Da (fragments). The reversed sequences of the target database were used as decoy database. Peptide and protein hits were filtered at an FDR of 1% using a target-decoy strategy⁴². In addition, only proteins identified by at least two unique peptides were retained. Only proteins identified in at least two replicates were considered when comparing protein abundances between control and drug treatment.

To reduce technical variation, data were quantile-normalized using the preprocessCore library⁴³. Protein differential expression was evaluated using the limma package. Differences in protein abundances were statistically determined using the Student's *t*-test moderated by Benjamini–Hochberg's method⁴⁴ at an α level of 0.05. Significantly regulated proteins were defined by a cut-off of \log_2 fold change ≥ 2 and $P \leq 0.1$. Presented values are reached after imputing for not-missing-at-random from controls and correcting for an overall higher intensity in test samples in comparison to control samples. For gene ontology (GO) term and pathway enrichment analysis, significantly changed proteins were annotated using Blast2GO⁴⁵ with default parameters using the NCBI blast search. GO term enrichment was done within Blast2GO and significantly enriched (FDR-corrected $P < 0.05$) most specific GO terms were listed. For KEGG pathway enrichment analysis EC numbers from Blast2Go annotation were extracted and the EC2KEGG tool⁴⁶ was used to annotate respective species-specific KEGG pathways and perform enrichment analysis ($P < 0.05$).

Two-dimensional TPP and protein expression analysis

TPP was performed as previously described^{29,47}. In brief, cells were grown anaerobically at 37 °C for 48 h. Cells were then washed twice and the optical density was adjusted to 5. For whole-cell experiments, duloxetine was then added at five different concentrations and incubated for 30 min. For lysate experiments, cells were disrupted with five freeze–thaw cycles before duloxetine treatment. Aliquots of treated cells or lysates were then heated for 3 min to ten different temperatures in a PCR machine (Agilent SureCycler 8800). After cell lysis, protein aggregates were removed and the remaining soluble proteins were collected.

For full proteome quantification, cells were inoculated at an OD_{578 nm} of 0.01 and duloxetine was added at five different concentrations. Cells were grown anaerobically for 48 h, washed twice with PBS and lysed as previously described⁴⁷.

Proteins from these experiments were digested according to a modified SP3 protocol^{48,49}, as previously described⁴⁷. Peptides were labeled with TMT10plex (Thermo Fisher Scientific), fractionated onto six fractions under high pH conditions and analysed with LC–MS/MS, as previously described⁴⁷. Protein identification and quantification was performed using IsobarQuant³⁰ and Mascot 2.4 (Matrix Science) against Uniprot Proteome (ID: UP000000625 for *E. coli* IAI1, UP000000748 for *E. coli* ED1a and UP000001662 for *C. saccharolyticum*). Data were analysed with the TPP package for R³⁰.

Secreted metabolite analysis (reverse phase LC–MS/MS, Orbitrap)

Bacterial cells from a 20-ml overnight culture were washed for use in resting cell and lysate assays as described below. The duloxetine concentration used was 1 mM and all interactions were tested in triplicate. For the resting cell assay, bacteria were reconstituted in 3.6 ml PBS, pH 6.5 containing 1 mM MgCl₂; the sample volume was 600 µl. For the

lysate assay, bacteria were reconstituted in 1 ml PBS, lysed, and then 360 µl of the recovered lysate diluted with 1,080 µl PBS, thus the final sample volume for each replicate (six in total; three drug and three control) was 240 µl. Resting cells were incubated for 2 h and lysates for 30 min with duloxetine or with DMSO as control. As another control, buffer with duloxetine was incubated for the respective time in the respective sample volume. Cells and lysate were centrifuged (14,000 rpm, 10 min, 4 °C) and only the supernatant was extracted (450 µl for resting cells, and 187.5 µl in case of lysates) in ice-cold 1:1 methanol:acetonitrile containing 10 µM amitriptyline as an internal standard. Samples were vacuum-dried, and reconstituted in 20% acetonitrile containing 250 µM caffeine as an additional internal standard. Resting cell samples were reconstituted in 225 µl reconstitution buffer, doubling the respective concentration of small molecules in comparison to the original sample. Lysate samples were reconstituted in 187.5 µl; the concentration in comparison to the original culture remained constant.

Samples were measured on a Q Exactive Plus-Orbitrap Mass Spectrometer (Thermo Fisher Scientific) in positive mode using a Kinetex C18 column (30 × 2.1 mm, 2.6 µm, 100 Å) for liquid chromatography kept at room temperature. Mobile phase A: 5 mM formic acid in water:acetonitrile 98:2 (v/v); mobile phase B: 5 mM formic acid in water:acetonitrile 2:98 (v/v). Five microlitres of sample was injected at 95% mobile phase A, maintained for 3 min, followed by a linear gradient up to 98% B in 20 min, maintained for 7 min, followed by a linear gradient up to 95% A over 1 min, which was maintained for 3 min. The flow rate was 0.3 ml min⁻¹. Samples were injected in three rounds representing three technical replicates including one washing injection every ten injections. The scan mode was FTMS + p ESI Full ms and the scan range was 60–800 m/z. Resolution was set to 70,000, AGC target to 1,000,000 ions and maximum IT to 150 ms. For secondary MS the resolution was set to 17,500, AGC target to 100,000 ions and maximum IT to 60 ms, allowing five secondary scans ranging from 200 to 2,000 m/z per full scan at a collision energy of 35 eV. Unknown charges or charges higher than 2 were excluded from analysis. Ions with small fold changes were filtered out as described previously⁵⁰.

Raw data were converted from Thermo Fisher Scientific .raw format into the open mzXML format using RawConverter⁵¹. For feature selection, peak alignment, grouping and retention time shift correction from the raw data the XCMS R package was used^{52,53}. Parameters for the first round of density grouping of peaks were bw = 30, minfrac = 0.5, minsamp = 3, mzwid = 0.025, max = 50. For retention time correction, parameters were family = "symmetric", plottype = "mdevden". For second round of grouping, parameters were bw=10, minfrac = 0.5, minsamp = 3, mzwid = 0.025, max = 50. Missing peaks were filled using the 'chrom' method. Statistical analysis was based on three biological replicates with two technical replicates each. Statistical analysis was based on previous work^{50,54}. Mapping to the databases METLIN⁵⁵ and KEGG⁵⁶ were based on 10 ppm accuracy. Only H⁺ and [ACN + H]⁺ adducts were considered. For comparison between samples, all features were normalized using amitriptyline internal standard (*m/z* 278.18). For four of the metabolites (guanosine, inosine, xanthine, and hypoxanthine), retention times and MS/MS matches against internal standards were used for annotation (Extended Data Fig. 6e–h).

Clostridium saccharolyticum secreted metabolite validation (reverse-phase LC–MS/MS, Q-ToF)

Bacterial cells were cultivated and treated with duloxetine as in the previous section. Cells were centrifuged (14,000 rpm, 10 min, 4 °C) and 900 µl of the supernatant was extracted with 2,700 µl ice-cold 1:1 methanol:acetonitrile. After centrifugation (14,000 rpm, 10 min, 4 °C), 3,500 µl of the extracted metabolites were dried under vacuum (Savant DNA 120 SpeedVac concentrator, Thermo Fisher Scientific, with the following options: medium drying rate and heat option inactivated). Samples were reconstituted in 150 µl of 20% acetonitrile containing 10 µg ml⁻¹ caffeine as an internal standard. Analytical standards for

selected metabolites (xanthine, inosine, guanosine, adenosine and hypoxanthine) were reconstituted in 150 µl of 20% acetonitrile at a final concentration of 10 µg ml⁻¹.

Chromatographic separation was achieved using an Agilent Zorbax SB-C18 column (2.1 mm × 100 mm, 1.8 µm) attached to an Agilent 1290 Infinity LC system coupled to Agilent 6546 LC/Q-ToF. Column temperature was maintained at 40 °C. Mobile phase A consisted of 5 mM ammonium formate in water with 0.1% formic acid, and mobile phase B consisted of 5 mM ammonium formate in methanol with 0.1% formic acid. One microlitre of sample was injected at 95% mobile phase A, followed by a linear gradient up to 30% mobile phase B over one minute, followed by a linear gradient up to 100% mobile phase B over 7 min, which was maintained for one minute. Post-run equilibration was achieved over 4 min. The flow rate was 0.2 ml min⁻¹.

The Agilent 6546 LC/Q-ToF was operated with the following source parameters: gas temperature, 200 °C; gas flow 9 l min⁻¹; nebulizer 35 psig; sheath gas temperature 400 oC; sheath gas flow 12 l min⁻¹; Vcap 2500 V; nozzle voltage 0 V; fragmentor 120 V; skimmer 145 V; octupole RF peak 750. The instrument was operated in negative mode with the selection of the targeted MS/MS option for the following *m/z*: 151.0261 (xanthine, [M – H]⁻), 267.0734 (inosine, [M – H]⁻), 282.0841 (guanosine, [M – H]⁻), 266.089 (adenosine, [M – H]⁻) and 135.0312 (hypoxanthine, [M – H]⁻). The isolation width was set to medium (around 4 amu), the collision energy to 10 eV and the acquisition time to 200 ms per spectra. The *m/z* range for MS and MS/MS was set to 50–500. Online mass calibration was performed using a second ionization source and a constant flow (2 ml min⁻¹) of reference solution (119.0363 and 1,033.9881 *m/z*). For data analysis, the MassHunter Qualitative Analysis Software (Agilent, v.10.0) was used. Metabolite identification of xanthine, inosine, guanosine and hypoxanthine in samples was performed by matching the retention time, the precursor *m/z* and the fragment ions *m/z* with the ones from the respective analytical standards (Supplementary Table 11).

Secreted metabolite analysis (FIA–MS, Orbitrap)

Untargeted metabolomics analysis was performed as described previously^{57,58}. In brief, samples were analysed on a platform consisting of a Thermo Scientific Ultimate 3000 liquid chromatography system with autosampler temperature set to 10 °C coupled to a Thermo Fisher Scientific Q-Exactive Plus Fourier transform mass spectrometer equipped with a heated electrospray ion source and operated in negative ionization mode. The isocratic flow rate was 150 µl min⁻¹ of mobile phase consisting of 60:40% (v/v) isopropanol:water buffered with 1 mM ammonium fluoride at pH 9 and containing 10 nM taurocholic acid and 20 nM homotaurine as lock masses. Mass spectra were recorded in profile mode from 50 to 1,000 *m/z* with the following instrument settings: sheath gas, 35 arbitrary units (AU); aux gas, 10 AU; aux gas heater, 200 °C; sweep gas, 1 AU; spray voltage, -3 kV; capillary temperature, 250 °C; S-lens RF level, 50 AU; resolution, 70,000 at 200 *m/z*; AGC target, 3 × 10⁶ ions; maximum inject time, 120 ms; acquisition duration, 60 s. Spectral data processing was performed using an automated pipeline in R as described previously⁵⁷. Detected ions were tentatively annotated as metabolites on the basis of matching accurate mass within a tolerance of 5 mDa using the Human Metabolome database⁵⁹ as reference.

Secreted metabolite analysis (HILIC–LC–MS and MS/MS, Q-ToF)

Liquid samples were prepared for LC–MS and LC–MS/MS analysis through the addition of an equal volume of ice cold (90:10) acetonitrile: 5 mM ammonium acetate (pH 9). Extractions were incubated for one hour at -20 °C followed by centrifugation at 4,500 rpm (2,850g) for 10 min at 4 °C. Twenty microlitres of extraction supernatant were transferred to Nunc 96-well, V-shape plates, closed with temperature-sensitive seals and stored at -80 °C until further analysis. Samples were analysed as previously reported (Agilent application note – 5994-1492EN). In brief, chromatographic separation was

Article

achieved using an Agilent InfinityLab Poroshell 120 HILIC-Z column, 2.1 mm × 150 mm, 2.7 µm column and an Agilent 1290 Infinity II LC system coupled to an Agilent 6550 Q-ToF mass spectrometer. Column temperature was maintained at 45 °C and the following mobile phases were used: mobile phase A: ammonium acetate 5 mM, pH 9, and 250 µM InfinityLab Deactivator; and mobile Phase B: ammonium acetate in acetonitrile:water 85:15 (v/v) 5 mM, pH 9, and 250 µM InfinityLab Deactivator (Agilent). Five microlitres of sample was injected at 96% mobile phase B, maintained for 2 min, followed by a linear gradient up to 88% B in 3.5 min, maintained for 3 min, followed by a linear gradient to 86% B in 0.5 min and maintained at 86% for 5 min, then a linear gradient to 82% mobile phase B over 3 min, and a linear gradient to 65% B over 5 min, which was maintained for 1 min. The column was allowed to re-equilibrate HILIC conditions for 8 min before each sample injection. The flow rate was 0.25 ml min⁻¹. The Q-ToF was operated in negative scanning mode (60–1,600 *m/z*) with the following source parameters: VCap, 3,500 V; nozzle voltage, 0 V; gas temperature, 225 °C; drying gas 13 l min⁻¹; nebulizer, 35 psi; sheath gas temperature 350 °C; sheath gas flow 12 l min⁻¹, fragmentor, 125 V and skimmer, 45 V. Online mass calibration was performed using a second ionization source and a constant flow (10 µl min⁻¹) of reference mass solution (119.0363 and 1033.9881 *m/z*).

LC–MS/MS analysis was performed using the same chromatographic separation conditions and source parameters described above, but using an Agilent 6546 Q-ToF mass spectrometer, allowing operation in auto-MS/MS mode with iterative selection of a preferred inclusion list of parent ions. Parent ions for tandem mass spectrometry analysis were selected from the LC–MS data described above using 20 ppm mass tolerance and 0.5 min retention time tolerance, iso width set to ‘narrow width’ and collision energy to 10, 20 and 40 eV.

The MassHunter Qualitative Analysis Software (Agilent Technologies, v.10.0) was used for both LC–MS and LC–MS/MS molecular feature extraction. The following settings were applied: peak filter of absolute height: 5,000 counts, limit assigned charge states to 1, only H⁺ charged molecules were included and compound quality score cut-off was set to be greater than 80%. Peak alignment was carried out using Mass Profiler Professional (Agilent, v.15.1) with default parameters: mass tolerance of 2 mDa or 20 ppm and retention time tolerance of 0.3 min or 2%. A standard organic molecule model (MassHunter v.10.0, Agilent) was used to de-isotope compounds and features were only extracted when at least two matching isotopes (retention time and relative abundance) could be detected. Only [M – H]⁻ ions were considered for annotations. Extracted and aligned compounds were putatively annotated using the Metlin PCDL B.08.0 metabolite and peptide database/library, by using mass tolerance of 20 ppm.

For putative metabolite identification, cosine spectral similarity was computed for all the available collision energies using the Spectrum-Similarity function using OrgMassSpecR-v0.5-3 (<https://cran.r-project.org/web/packages/OrgMassSpecR/index.html>). The *m/z* tolerance for alignment was set to default (0.25). When multiple collision energies were available (both reference and measured), the one showing the highest spectral similarity score was retained. Molecules showing similarity score above 0.5 were assigned Metabolomics Standards Initiative (MSI)⁶⁰ ID level 2; molecules showing a spectral similarity score below 0.5 were assigned MSI ID level 3. MSI ID level 2 matches are shown in Supplementary Fig. 2. MSI level 1 assignment was made for linolenic acid and glycocholic acid on the basis of accurate mass and retention time comparison with chemical standards (Supplementary Fig. 3, Supplementary Table 17).

Cross-feeding candidate ion identification

Ions (*m/z* features) that were: (i) not present in the starting medium; (ii) increased during *S. salivarius* growth in the presence of duloxetine; and (iii) decreased during *E. rectale* growth were chosen as hits. Ions showing these characteristics in the DMSO (solvent) control were filtered out.

Community assembly assay

Oversight anaerobic cultures of the five bacterial species were inoculated in 2 ml GMM with 50 µM duloxetine to initial total cell concentration corresponding to an optical density of 0.1. Roughly equal amounts, by optical density, were used from each of the five monocultures. Tubes were incubated for 48 h anaerobically at 37 °C without shaking. For DNA extraction, 1 ml of culture was centrifuged for 10 min at 14,000 rpm in 1.5-ml Eppendorf tubes. The bacterial pellet was frozen at –80 °C until DNA extraction. For drug extraction, 600 µl of cold ACN:methanol was added to the supernatant and incubated for 15 min in the fridge. Samples were then centrifuged for 10 min, 14,000 rpm at 4 °C, and 700 µl was transferred to a new tube and dried in a speedvac (Eppendorf Vacuum Concentrator Plus) for 5 h at 30 °C at V-AL mode. For UPLC measurement, the samples were reconstituted in 116 µl 20% ACN containing 250 µM caffeine as an internal standard.

DNA extraction and 16S barcode sequencing library preparation. Bacteria pellets were dissolved in lysis buffer and transferred into a 96 Polypropylene Deep Well plate (3959, Corning). An in-house protocol was used for DNA extraction. Specifically, the GNOME DNA isolation Kit (MP Biomedicals) was adapted to be used with the Biomek FXp Liquid Handling Automation Workstation (Beckman). Subsequently, purified DNA was obtained using ZR-96 DNA Clean & Concentrator TM-5 (D4024, Zymo Research). After the integrity of the DNA was verified by agarose gel electrophoresis, the DNA concentration of the samples was determined using the Qubit dsDNA BR assay kit (Q32850, Life Technologies) in combination with the Infinite M1000 PRO plate reader (Tecan). The 16S V4 amplicons were generated using an Illumina-compatible two-step PCR protocol: in the first PCR the 16S V4 region was amplified with the primers F515/R806⁶¹; and then in the second PCR barcode sequences were introduced using the NEXTflex 16S V4 Amplicon-Seq Kit (4201-05, Bioo Scientific). After multiplexing equal volumes of PCR products from each sample, the SPRIselect reagent kit (B23318, Beckman Coulter) was used for left-side size selection. Before Illumina sequencing, the quality of the library was checked by the 2100 BioAnalyzer (Agilent Technologies) and the DNA concentration was determined using the Qubit dsDNA HS assay kit. Sequencing was performed using a 250-bp paired-end sequencing protocol on the Illumina MiSeq platform (Illumina) at the Genomics Core Facility (EMBL Heidelberg).

16S barcode sequencing analysis. The raw Illumina paired-end reads were quality-trimmed and length-filtered using Cutadapt with a quality threshold of 30 bp and length cut-off of 150 bp. The amplicon sequences were compared to the 16S rRNA gene of the species mixed for coculture using UCLUST⁶². Only those that have a minimum of 98% identity were clustered into the operational taxonomic units. The species abundance was normalized by the 16S rRNA gene copy numbers.

Conditioned medium assay

The supernatant of cultures of *S. salivarius* treated with 50 µM duloxetine or an equivalent amount of DMSO (solvent control) were filtered with a Millipore 0.22-µm filter after centrifugation. To additionally account for the effect of duloxetine on bacterial growth, duloxetine was added to the supernatant from the untreated control to a concentration of 50 µM. The resulting conditioned medium or spent medium control were inoculated with *E. rectale* at an OD_{578 nm} of 0.01 and the growth was measured by following the optical density. Experiments were performed in triplicate.

Caenorhabditis elegans duloxetine interaction assays

Bacteria were incubated with duloxetine as follows: 0.5 ml of overnight bacterial culture (or lysogeny broth (LB) only for controls) was added to 4.5 ml LB and shaken for 2 h at 37 °C, after which duloxetine was added and shaking continued for a further 22 h. Cultures were centrifuged at 4,500 rpm for 10 min and supernatant was sterilized by passing

through a 0.22- μ m filter. *C. elegans* N2 wild type was maintained in nematode growth medium (NGM), as previously described⁶³. Worms at the L4 larval stage raised on NGM plates containing *E. coli* BW25113 bacteria were washed three times in M9. Fifty worms per 100 μ l of control LB medium with DMSO, LB medium with duloxetine at 0, 0.1, 0.5 and 1 mM or spent LB medium from *E. coli* IAI1 or ED1a were added to a 96-well flat-bottom microtitre plate. Assay plates were incubated at 20 °C for 60 min, with regular shaking at 140 rpm, and the number of regular moving worms (displaying movement at least once every 3 s) was counted and expressed as a percentage of total worms per well.

Replicates and statistical tests

Technical replicates refer to replicates within the same batch (for example, three bacterial cultures inoculated from the same starting culture), whereas biological replicates refer to independent experiments. All indicated sample numbers (or displayed data points) refer to distinct samples (biological replicates) and not to repeated measurements of the same samples. All statistical tests are two-sided. FDR corrections were performed using the Benjamini–Hochberg procedure.

Reporting summary

Further information on research design is available in the Nature Research Reporting Summary linked to this paper.

Data availability

All data generated during this study are included in this published Article (and its Supplementary Information files). Supplementary Table 18 provides an overview of the different methods and data associated with all figures. UPLC and mass spectrometry data are deposited at the Metabolights repository under the accession codes MTBLS1264, MTBLS1757, MTBLS1627, MTBLS1319, MTBLS1791, MTBLS1792, and MTBLS2885. The mass spectrometry proteomics data have been deposited to the ProteomeXchange Consortium with the dataset identifiers PXD016062 and PXD016064. Source data are provided with this paper.

Code availability

The data analysis codes are available at https://github.com/sandrejev/drugs_bioaccumulation.

40. Cox, J. & Mann, M. MaxQuant enables high peptide identification rates, individualized p.p.b.-range mass accuracies and proteome-wide protein quantification. *Nat. Biotechnol.* **26**, 1367–1372 (2008).
41. Cox, J. et al. Andromeda: a peptide search engine integrated into the MaxQuant environment. *J. Proteome Res.* **10**, 1794–1805 (2011).
42. Elias, J. E. & Gygi, S. P. Target–decoy search strategy for increased confidence in large-scale protein identifications by mass spectrometry. *Nat. Methods* **4**, 207–214 (2007).
43. Gentleman, R. C. et al. Bioconductor: open software development for computational biology and bioinformatics. *Genome Biol.* **5**, R80 (2004).
44. Benjamini, Y. & Hochberg, Y. Controlling the false discovery rate: a practical and powerful approach to multiple testing. *J. R. Stat. Soc. B* **57**, 289–300 (1995).
45. Conesa, A. et al. Blast2GO: a universal tool for annotation, visualization and analysis in functional genomics research. *Bioinformatics* **21**, 3674–3676 (2005).
46. Porollo, A. EC2KEGG: a command line tool for comparison of metabolic pathways. *Source Code Biol. Med.* **9**, 19 (2014).
47. Mateus, A. et al. Thermal proteome profiling in bacteria: probing protein state in vivo. *Mol. Syst. Biol.* **14**, e8242 (2018).
48. Hughes, C. S. et al. Ultrasensitive proteome analysis using paramagnetic bead technology. *Mol. Syst. Biol.* **10**, 757 (2014).
49. Hughes, C. S. et al. Single-pot, solid-phase-enhanced sample preparation for proteomics experiments. *Nat. Protoc.* **14**, 68–85 (2019).

50. Ortmayr, K., Charwat, V., Kasper, C., Hann, S. & Koellensperger, G. Uncertainty budgeting in fold change determination and implications for non-targeted metabolomics studies in model systems. *Analyst* **142**, 80–90 (2017).
51. He, L., Diedrich, J., Chu, Y. Y. & Yates, J. R. 3rd Extracting accurate precursor information for tandem mass spectra by RawConverter. *Anal. Chem.* **87**, 11361–11367 (2015).
52. Mahieu, N. G., Generbacher, J. L. & Patti, G. J. A roadmap for the XCMS family of software solutions in metabolomics. *Curr. Opin. Chem. Biol.* **30**, 87–93 (2016).
53. Smith, C. A., Want, E. J., O’Maille, G., Abagyan, R. & Siuzdak, G. XCMS: processing mass spectrometry data for metabolite profiling using nonlinear peak alignment, matching, and identification. *Anal. Chem.* **78**, 779–787 (2006).
54. Vinaixa, M. et al. A guideline to univariate statistical analysis for lc/ms-based untargeted metabolomics-derived data. *Metabolites* **2**, 775–795 (2012).
55. Smith, C. A. et al. METLIN: a metabolite mass spectral database. *Ther. Drug Monit.* **27**, 747–751 (2005).
56. Tanabe, M. & Kanehisa, M. Using the KEGG database resource. *Curr. Protoc. Bioinformatics* **38**, 112.1–112.43 (2012).
57. Fuhrer, T., Heer, D., Begemann, B. & Zamboni, N. High-throughput, accurate mass metabolome profiling of cellular extracts by flow injection-time-of-flight mass spectrometry. *Anal. Chem.* **83**, 7074–7080 (2011).
58. Ponomarova, O. et al. Yeast creates a niche for symbiotic lactic acid bacteria through nitrogen overflow. *Cell Syst.* **5**, 345–357 (2017).
59. Wishart, D. S. et al. HMDB 4.0: the human metabolome database for 2018. *Nucleic Acids Res.* **46**, D608–D617 (2018).
60. Summer, L. W. et al. Proposed minimum reporting standards for chemical analysis. Chemical Analysis Working Group (CAWG) Metabolomics Standards Initiative (MSI). *Metabolomics* **3**, 211–221 (2007).
61. Caporaso, J. G. et al. Global patterns of 16S rRNA diversity at a depth of millions of sequences per sample. *Proc. Natl Acad. Sci. USA* **108**, 4516–4522 (2011).
62. Edgar, R. C. Search and clustering orders of magnitude faster than BLAST. *Bioinformatics* **26**, 2460–2461 (2010).
63. Brenner, S. The genetics of *Caenorhabditis elegans*. *Genetics* **77**, 71–94 (1974).
64. Kanehisa, M. et al. Data, information, knowledge and principle: back to metabolism in KEGG. *Nucleic Acids Res.* **42**, D199–D205 (2014).

Acknowledgements This project was supported by the European Union’s Horizon 2020 research and innovation programme under the grant agreement number 686070, and by the UK Medical Research Council (project number MC_UU_00025/11). A.M., L.M., M.T. and V.P. were supported by the EMBL interdisciplinary postdoctoral program. We thank EMBL Genomics, Metabolomics and Proteomics core facilities for their support in respective analyses.

Author contributions M. Klünemann, P.B., A.T. and K.R.P. conceived the study. M. Klünemann, S.A., A.T. and K.R.P. planned the overall experiments. S.A. performed the overall data analysis. K.Z. and V.P. performed the drug clustering. M. Klünemann carried out the interaction screen, large-volume validation and UPLC data analysis. A.R.B., L.M., M.T. and M. Banzhaf assisted with the screen set-up. F.H. and C.S. designed and synthesized the clickable drug. M. Klünemann, M.-T.M. and T.B. performed the click chemistry proteomics experiments. M. Beck designed and supervised the click chemistry proteomics analysis. A.M. and M.M.S. planned the TPP experiments. S.B. and A.M. performed the TPP experiments. A.M., M.M.S. and S.A. analysed the TPP data. J.V. and D.C.S. performed the FIA-MS experiments and data analysis. S.B. performed the bacterial culturing experiments and P.P. performed the LC-MS analysis for drug measurements. M. Klünemann and P.P. performed the secreted metabolite LC-MS analysis in buffer. M. Klünemann and S.B. prepared the samples for, and B.S., L.N. and J.H. performed, the NMR analysis. M. Klünemann and D.K. performed growth assays and sample preparation for cross-fed metabolite analysis. S.B. performed growth assays and sample preparation for secreted metabolite analysis in GMM. S.D., E.M., E.K. and M.Z. performed the HILIC-MS/MS analysis. K.Z. analysed the cross-feeding metabolomics data. M. Kumar performed the motif analysis. M. Klünemann performed the community assembly experiments and Y.K. analysed the 16S data. T.A.S. and F.C. performed the *C. elegans* experiments and data analysis. D.K. measured drug concentrations. M. Klünemann and K.R.P. wrote the paper.

Competing interests M. Klünemann, S.A., L.M., M.T., Y.K., P.B., A.T. and K.R.P. are inventors in a patent application based on the findings reported in this study (US patent application number 16966322). S.B., A.M., P.P., S.D., J.V., B.S., T.A.S., E.K., D.K., K.Z., E.M., M. Banzhaf, M.-T.M., F.H., L.N., A.R.B., T.B., V.P., M. Kumar, C.S., M. Beck, J.H., M.Z., D.C.S., F.C. and M.M.S. declare no competing interests.

Additional information

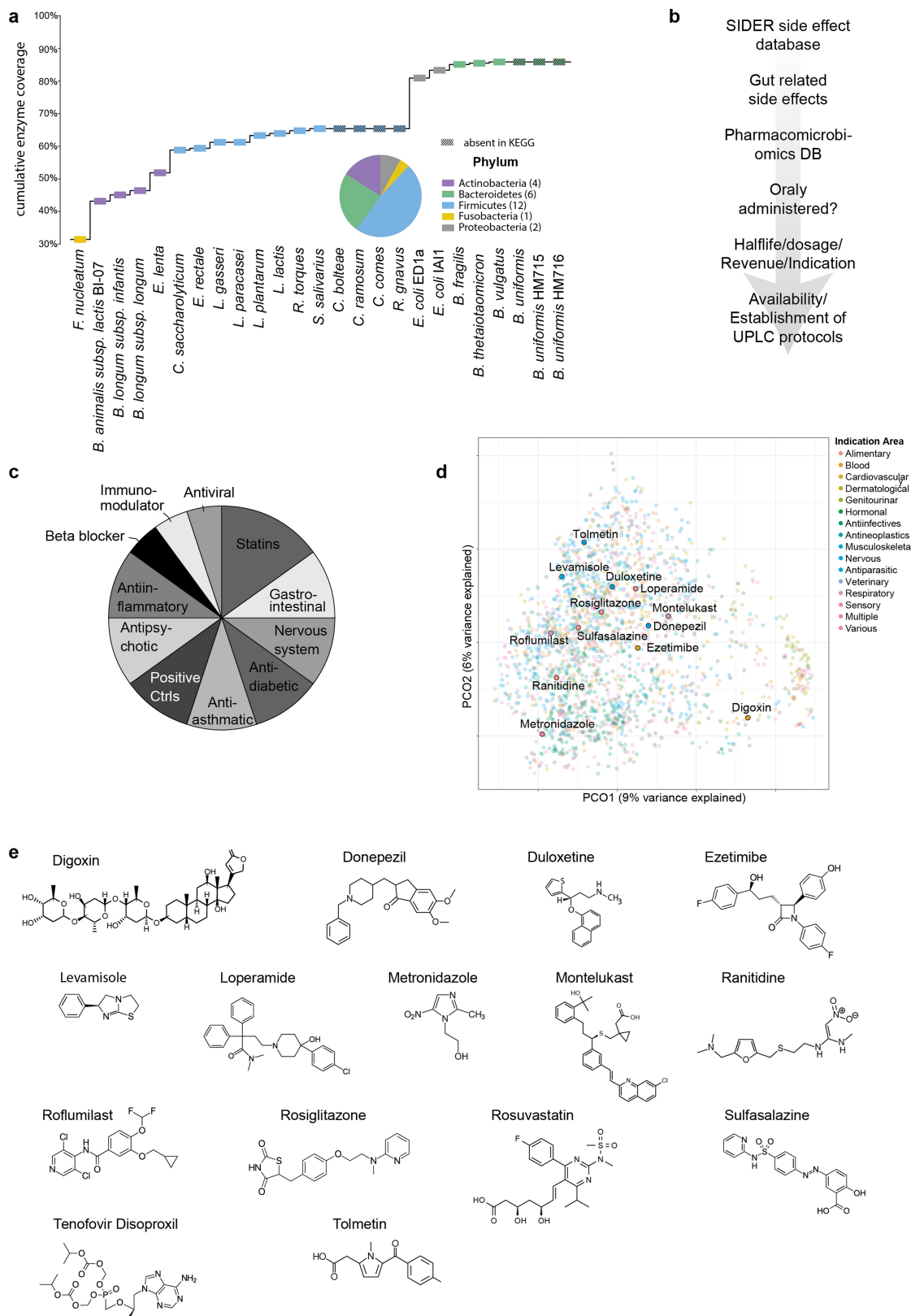
Supplementary information The online version contains supplementary material available at <https://doi.org/10.1038/s41586-021-03891-8>.

Correspondence and requests for materials should be addressed to Peer Bork, Athanasios Typas or Kiran R. Patil.

Peer review information *Nature* thanks Kim Lewis, Michael Shapira and the other, anonymous, reviewer(s) for their contribution to the peer review of this work.

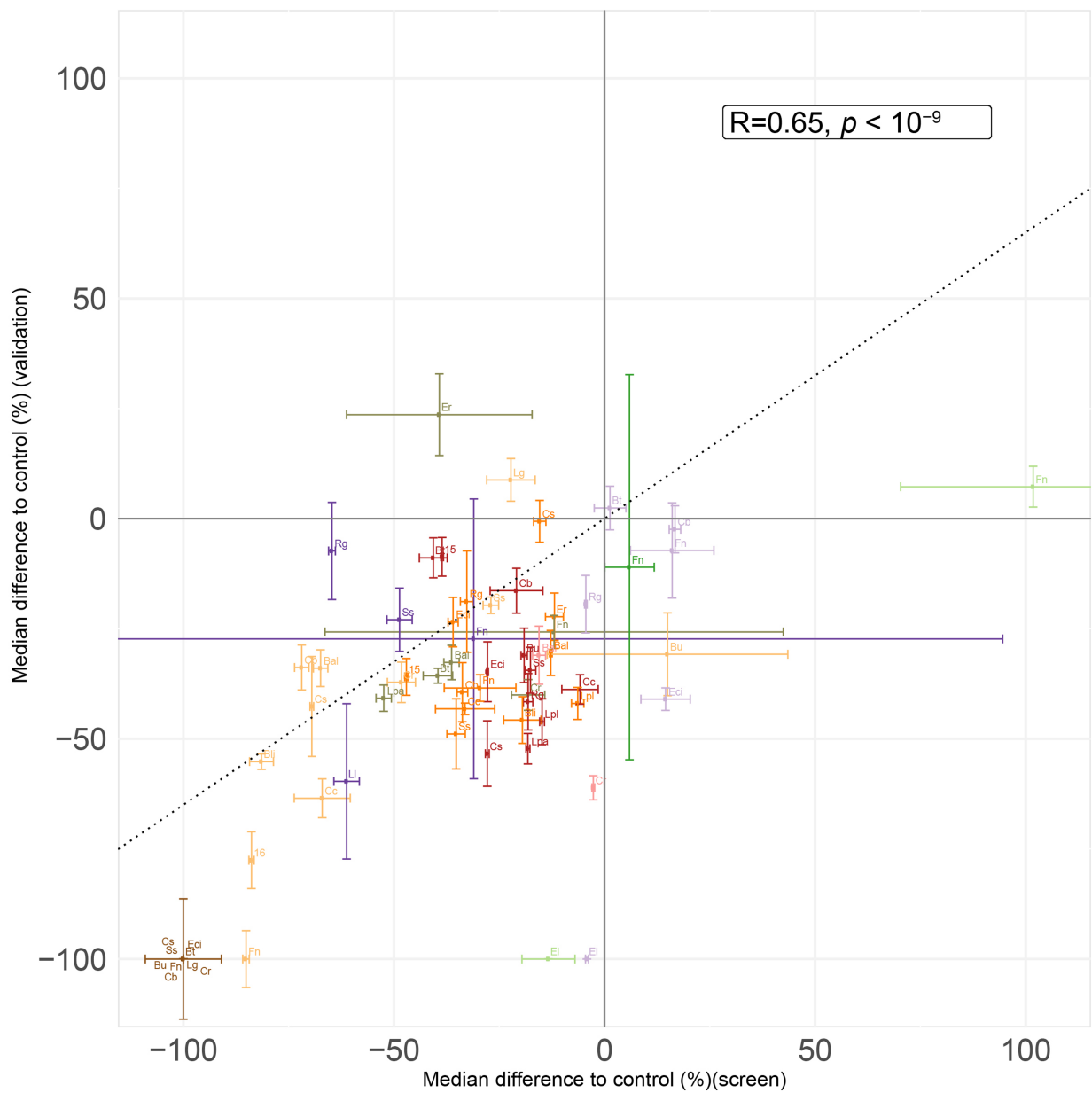
Reprints and permissions information is available at <http://www.nature.com/reprints>.

Article



Extended Data Fig. 1 | Bacteria and drug selection. **a**, Distribution of the selected 25 bacterial strains by their phylogenetic class, and their cumulative metabolic diversity measured as the coverage of annotated enzymes as per the KEGG database⁶⁴. **b**, We started with approximately 1,000 annotated drugs from the SIDER side effect database (Kuhn et al. 2016), which were filtered for their gut related side effects. Drug selection was enriched from another database (Saad et al. 2012) for known or suspected interactions with the gut microbiome, before filtered for oral administration and manually curated for

overall interest. Final selection was filtered for availability from vendors and establishment of UPLC methods. **c**, The drugs used in this study span a broad range of structural diversity. Shown is the spread of the selected drugs in a principle coordinate analysis, covering >2,000 drugs from the DrugBank database. Maximum common sub-structure was used to calculate the distances between drug pairs. **d**, Selected drugs cover several therapeutic classes/indication areas. **e**, Chemical structures of the 15 drugs used in this study.



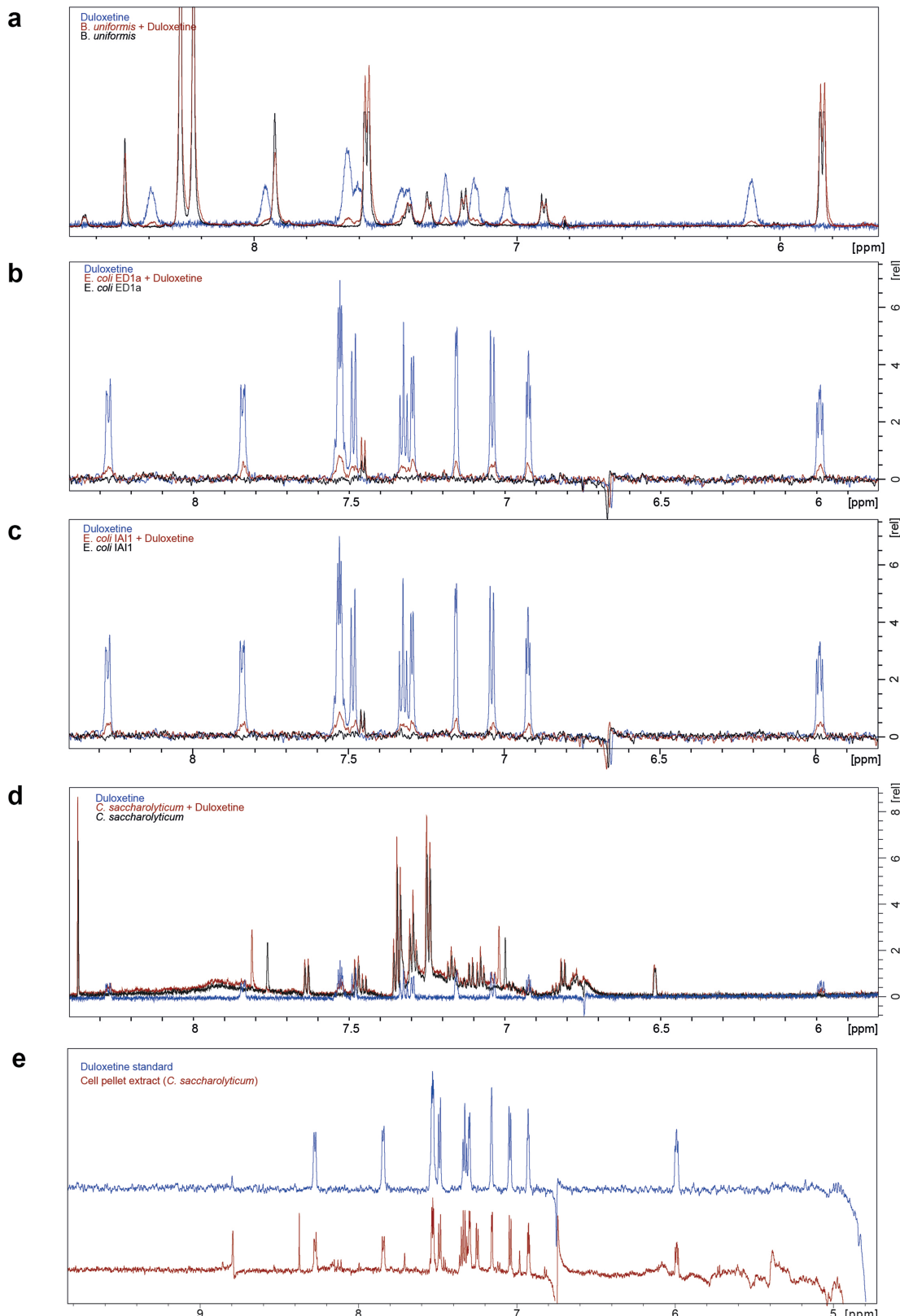
Drug Digoxin Donepezil Duloxetine Ezetimibe Levamisole Montelukast Ranitidine Roflumilast Rosiglitazone Sulfasalazine

- | | | | |
|---------|--|---------------------------------|----------------------------|
| Species | • 15: <i>B. uniformis</i> HM715 | • Cc: <i>C. comes</i> | • Lg: <i>L. gasseri</i> |
| | • 16: <i>B. uniformis</i> HM716 | • Cr: <i>C. ramosum</i> | • Li: <i>L. lactis</i> |
| | • Bal: <i>B. animalis</i> subsp. <i>lactis</i> BI-07 | • Cs: <i>C. saccharolyticum</i> | • Lpa: <i>L. paracasei</i> |
| | • Bli: <i>B. longum</i> subsp. <i>infantis</i> | • Eci: <i>E. coli</i> IAI1 | • Lpl: <i>L. plantarum</i> |
| | • Bt: <i>B. thetaiotaomicron</i> | • El: <i>E. lenta</i> | • Rg: <i>R. gnavus</i> |
| | • Bu: <i>B. uniformis</i> | • Er: <i>E. rectale</i> | • Ss: <i>S. salivarius</i> |
| | • Cb: <i>C. bolteae</i> | • Fn: <i>F. nucleatum</i> | |

Extended Data Fig. 2 | Correlation between the screen and validation in higher-volume cultures. For screen, $n \geq 4$ independent replicates (median number of replicates = 17). For validation, $n = 3$. Error bars = S.E.M. For

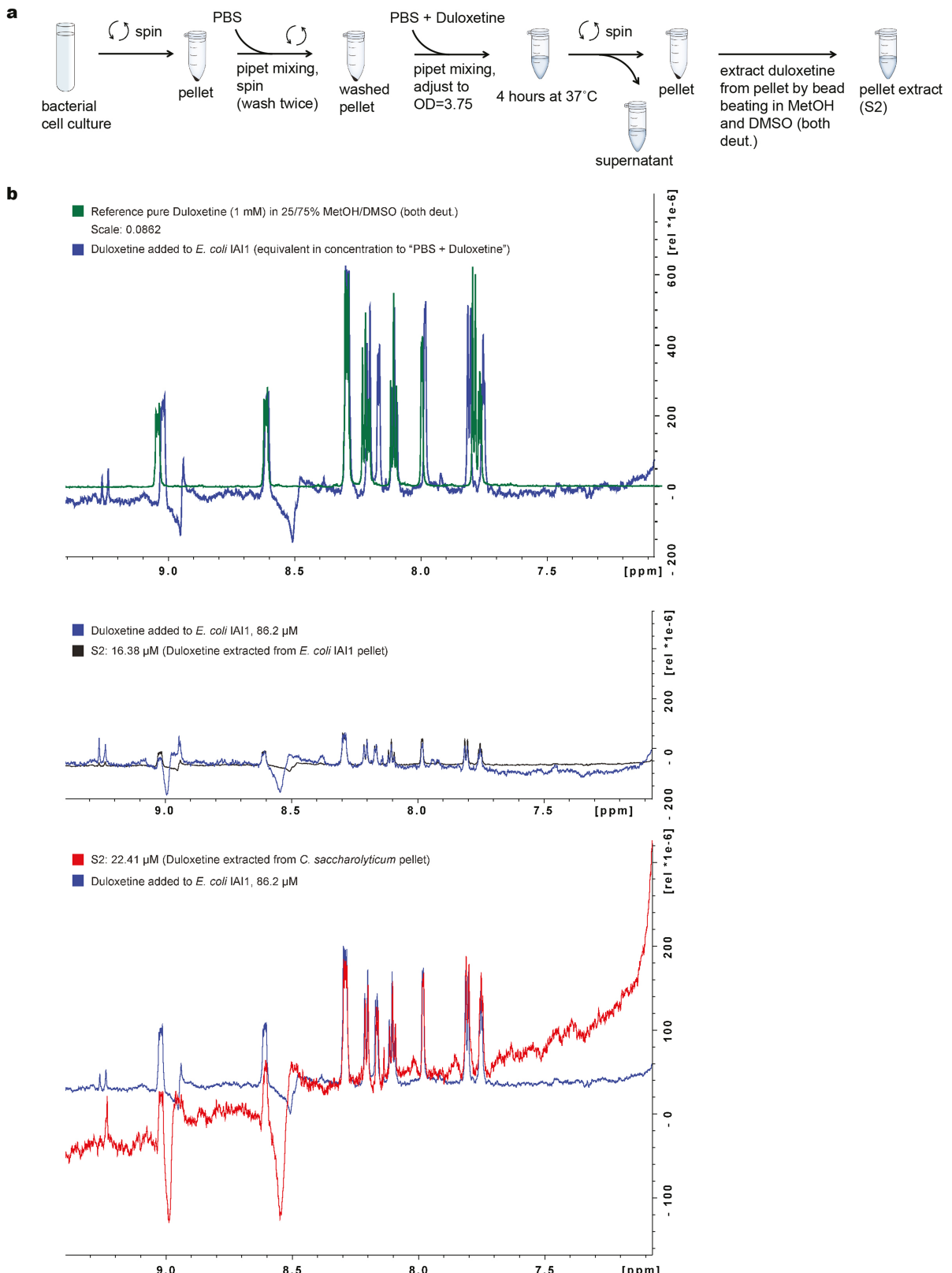
screening, multiple independent batches were performed as indicated in Supplementary Table 3. Shown R (correlation coefficient) and p-value based on Pearson correlation test.

Article



Extended Data Fig. 3 | NMR measurements showing duloxetine depletion by bacterial cells. **a, *B. uniformis*, b, *E. coli ED1A*, c, *E. coli IA1*, and d, *C. saccharolyticum*.** e, NMR spectrum from *C. saccharolyticum* cell pellet

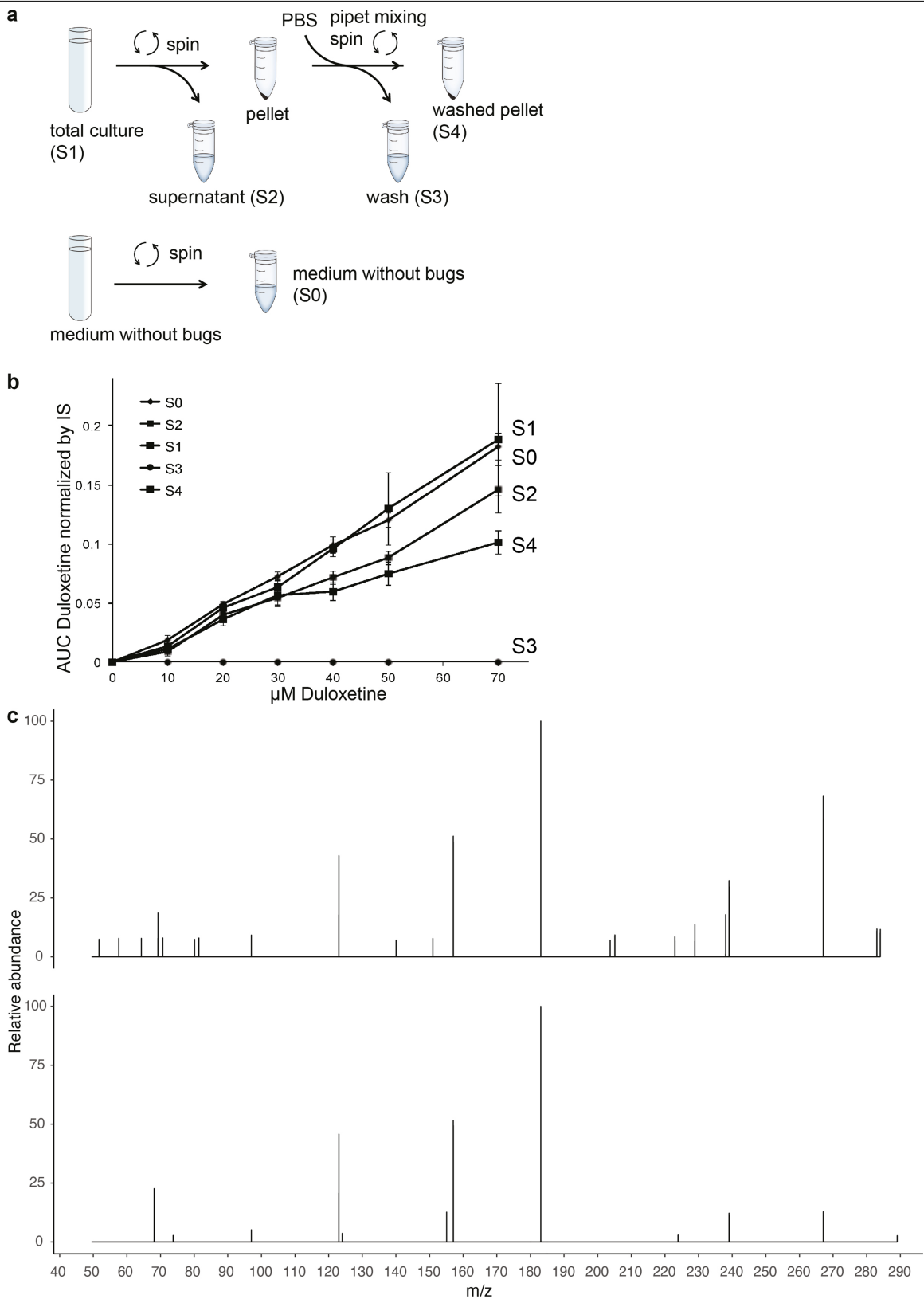
extract showing that the recovered drug is unmodified duloxetine. Resonances appearing to be out of phase and strong baseline distortions are due to the presence of large solvent signals outside the displayed chemical shift range.



Extended Data Fig. 4 | NMR measurements showing unmodified duloxetine recovered from bacterial pellet. Bacterial cells were incubated with the drug for 4 h in PBS buffer prior to recovery. **a**, Illustration of the experimental procedure marking the sample collection points. **b**, NMR spectra of recovered duloxetine from different fractions of *E. coli* IAI1 and *C. saccharolyticum*

preincubated in PBS. The reference spectrum was scaled to the amount present in the sample to assess the relative amount of free duloxetine present in respective samples. Resonances appearing to be out of phase and strong baseline distortions are due to the presence of large solvent signals outside the displayed chemical shift range.

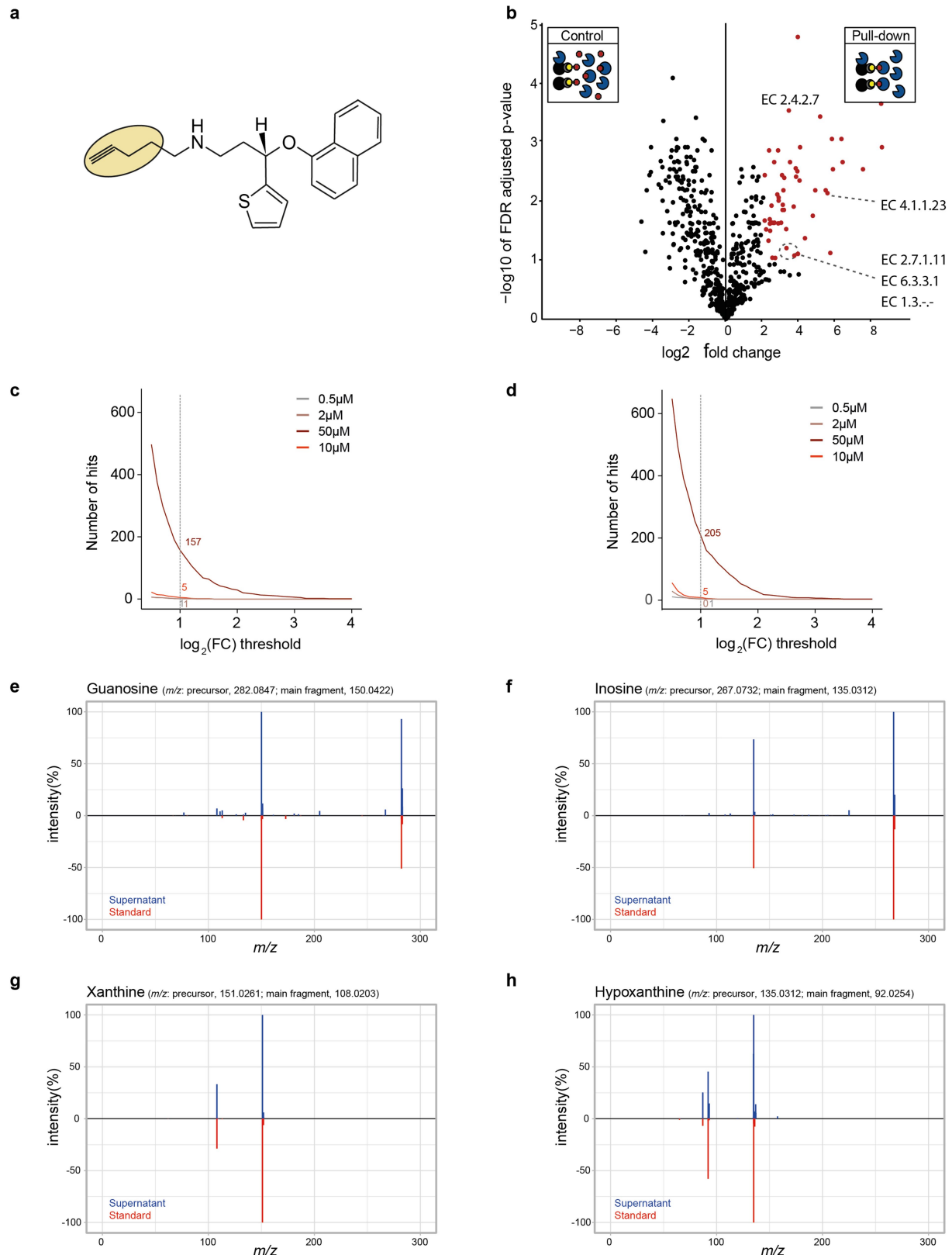
Article



Extended Data Fig. 5 | Duloxetine bioaccumulation by *E. coli* IAI1 in GMM and recovery from pellet. **a**, Procedure and collected samples: S0-S4.

b, Recovered duloxetine from different samples (S0-S4) collected as described in **a**. Different starting duloxetine concentrations, between 0-70 μ M, were used. S0 = medium without bacteria (drug only control), S1 = total culture

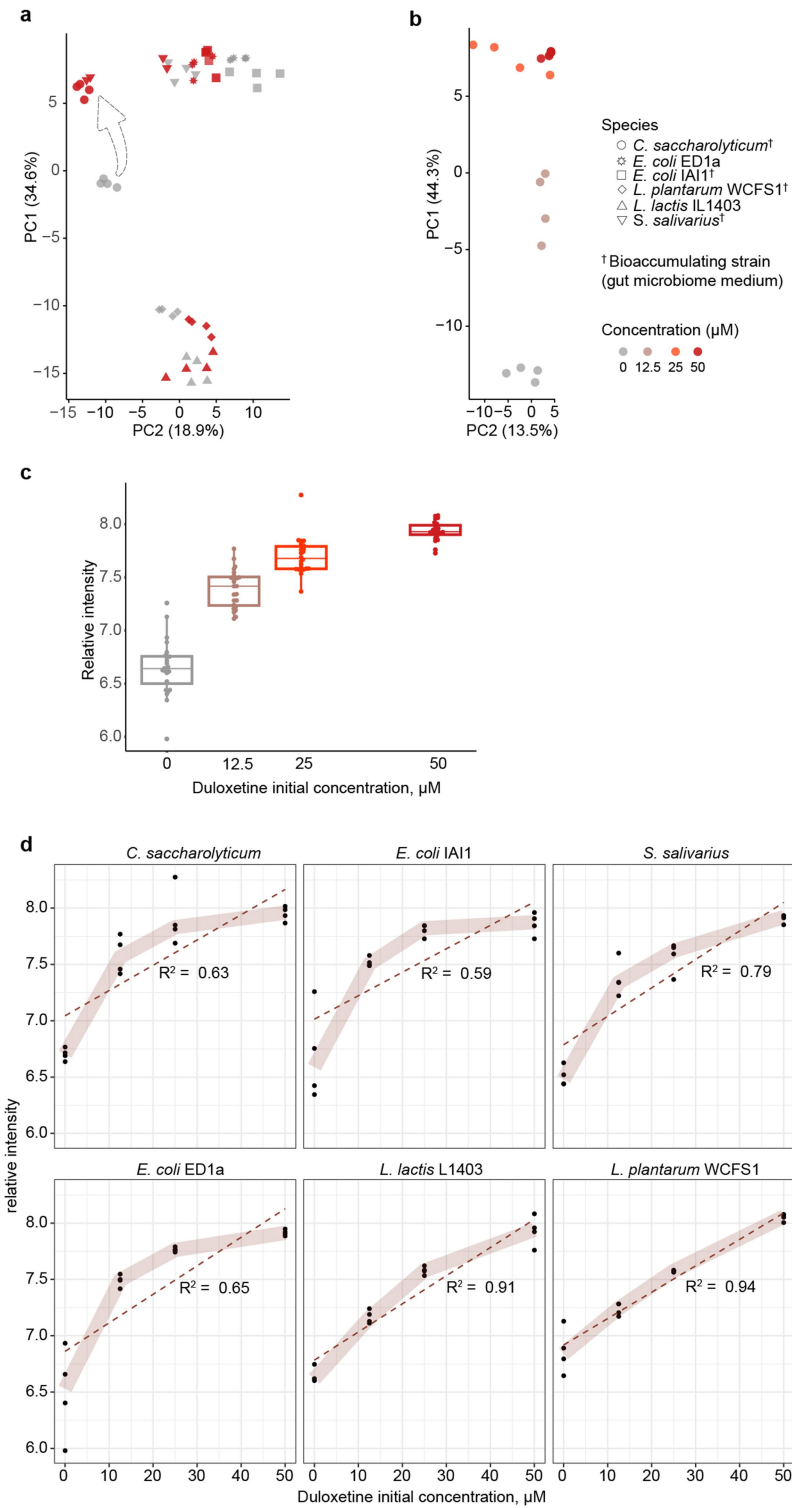
(medium plus bacteria), S2 = supernatant, S3 = wash (pellet was washed with PBS, no drug was found therein supporting intracellular accumulation), S4 = washed pellet. n = 3, error bars = SD, central squares mark the mean. **c**, MS/MS spectra of duloxetine standard (bottom) and duloxetine detected in a S1 sample (top).



Extended Data Fig. 6 | Molecular effects of duloxetine bioaccumulation.

a, Alkynated duloxetine made for the biotin-pull down assay. **b**, Fold change of proteins detected in the duloxetine pull down assay in *C. saccharolyticum* lysate using alkynated duloxetine. Four replicates were used in both test and control sets. Significantly enriched (hypergeometric test, FDR corrected $p < 0.1$, $\log_2(\text{FC}) > 2$) proteins are shown in red. **c**, **d**, Bioaccumulating *E. coli* strain features larger change in protein abundance in response to drug treatment.

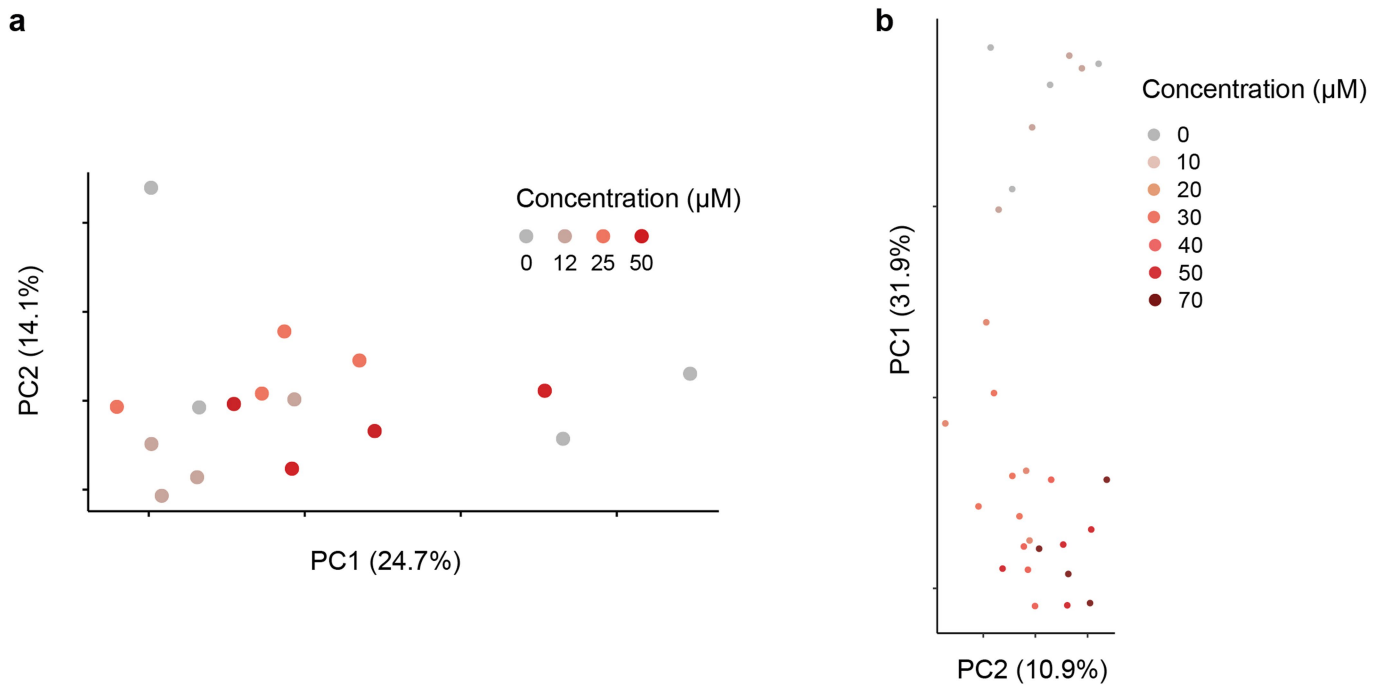
Show are the number of proteins with altered abundance in *E. coli* ED1A (**c**, non-bioaccumulating), and *E. coli* IAI1 (**d**, bioaccumulating) strains in response to duloxetine exposure at different concentrations. **e–h**, Comparison of MS/MS spectra of four nucleotide-pathway metabolites from the supernatant of duloxetine-treated *C. saccharolyticum* with MS/MS spectra of analytical standards. (CE = 10 eV; further details in Methods) Related to Fig. 2d and Supplementary Table 11.

**Extended Data Fig. 7 | Duloxetine induces a shift in metabolite secretion.**

a, Effect of duloxetine treatment on the exo-metabolome of six gut bacterial strains. Shown is the distribution of individual samples over the first two principle components. Principle Component Analysis (PCA) was performed on untargeted FIA-MS data (Methods). The numbers in parentheses of PC1 and PC2 mark the corresponding explained variance for the first and the second principle component, respectively. The dotted block arrow marks the duloxetine induced shift in exo-metabolome of *C. saccharolyticum*.

b, Duloxetine concentration dependent changes in the *C. saccharolyticum* exo-metabolome. The ion mapping to the deprotonated duloxetine was removed from the PCA analysis shown in **a** and **b**. **c**, The signal for the closest

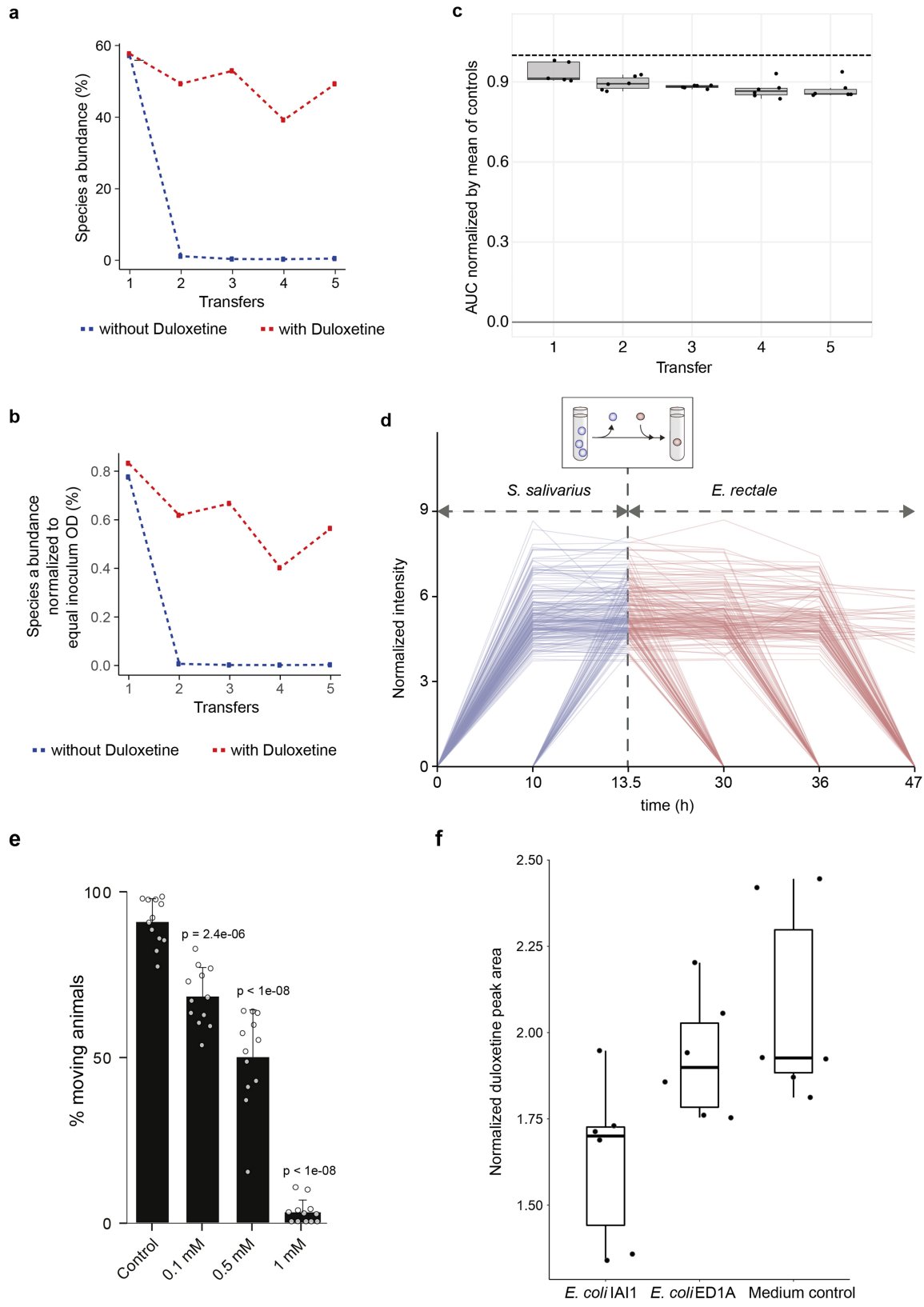
matching ion for deprotonated duloxetine [M-H]⁻ from the exometabolomics data (*m/z* 296.110079) plotted against initial duloxetine concentration. Data from all six species are pooled together (*n* = 24 for each initial duloxetine concentration). Overlaid box plots show the interquartile range (IQR), the median value and whiskers extending to include all the values less than $1.5 \times$ IQR away from the 1st or 3rd quartile, respectively. **d**, Duloxetine signal in the FIA-MS data stratified by species. The signal for the closest matching ion for deprotonated duloxetine [M-H]⁻ from the exometabolomics data (FIA-MS) (*m/z* 296.110079) plotted against initial duloxetine concentration. Thick transparent line traces medians of replicates (*n* = 4) at each initial concentration. The dotted lines show linear regression fit.



Extended Data Fig. 8 | Duloxetine-induced exo-metabolome changes.

a, Change in *C. saccharolyticum* exo-metabolome (HILIC-MS data) in response to non-bioaccumulated roflumilast. **b**, Same as in Fig. 2g, but based on 69

metabolites, whose chemical identity was putatively assigned, and confirmed for 2 metabolites using chemical standards (Supplementary Fig. 3, Supplementary Table 17), using HILIC-MS/MS analysis.



Extended Data Fig. 9 | See next page for caption.

Extended Data Fig. 9 | Duloxetine bioaccumulation, community assembly and host response. **a**, *E. rectale* relative abundance in transfer assays based on 16S amplicon reads. **b**, *E. rectale* relative abundance as in **a** but normalized with respect to equal abundance of each of the five species in the inoculum mixture. Mean values from biological triplicates are shown. **c**, Duloxetine depletion in community assembly assay. Dashed line indicates mean of control. $n = 6$ (3 biological replicates, 2 measurements per sample); overlaid box plots show the interquartile range (IQR), the median value and whiskers extending to include all the values less than $1.5 \times$ IQR away from the 1st or 3rd quartile, respectively. **d**, Metabolic cross-feeding between *S. salivarius* and *E. rectale*. Shown are the results of untargeted metabolomics analysis (FIA–MS) of supernatants collected during the growth of *S. salivarius* in GMM with duloxetine and the subsequent growth of *E. rectale* in the cell-free conditioned medium. Shown are the profiles of the ions that increased during *S. salivarius*

growth and decreased during *E. rectale* growth, implying cross-feeding. Ions showing similar pattern in the drug-free solvent (DMSO) control were filtered out. Mean intensities from three biological replicates are shown. **e**, Dose dependent effects of duloxetine on muscular function in wild type *C. elegans* animals. Larval stage four (L4) worms were incubated in LB medium in the presence of duloxetine at the indicated concentrations. Each bar represents the mean of six independent experiments, each performed with two technical replicates, \pm SD. *P* values mark difference to the no-drug control, estimated using one-way ANOVA followed by correction for multiple pair-wise comparisons (Tukey's test). **f**, Duloxetine concentration in the *C. elegans* behaviour assay ($n = 6$; 3 biological replicates, 2 measurements per sample). Overlaid box plots show the interquartile range (IQR), the median value and whiskers extending to include all the values less than $1.5 \times$ IQR away from the 1st or 3rd quartile, respectively.

Reporting Summary

Nature Research wishes to improve the reproducibility of the work that we publish. This form provides structure for consistency and transparency in reporting. For further information on Nature Research policies, see our [Editorial Policies](#) and the [Editorial Policy Checklist](#).

Statistics

For all statistical analyses, confirm that the following items are present in the figure legend, table legend, main text, or Methods section.

n/a Confirmed

- The exact sample size (n) for each experimental group/condition, given as a discrete number and unit of measurement
- A statement on whether measurements were taken from distinct samples or whether the same sample was measured repeatedly
- The statistical test(s) used AND whether they are one- or two-sided
Only common tests should be described solely by name; describe more complex techniques in the Methods section.
- A description of all covariates tested
- A description of any assumptions or corrections, such as tests of normality and adjustment for multiple comparisons
- A full description of the statistical parameters including central tendency (e.g. means) or other basic estimates (e.g. regression coefficient) AND variation (e.g. standard deviation) or associated estimates of uncertainty (e.g. confidence intervals)
- For null hypothesis testing, the test statistic (e.g. F , t , r) with confidence intervals, effect sizes, degrees of freedom and P value noted
Give P values as exact values whenever suitable.
- For Bayesian analysis, information on the choice of priors and Markov chain Monte Carlo settings
- For hierarchical and complex designs, identification of the appropriate level for tests and full reporting of outcomes
- Estimates of effect sizes (e.g. Cohen's d , Pearson's r), indicating how they were calculated

Our web collection on [statistics for biologists](#) contains articles on many of the points above.

Software and code

Policy information about [availability of computer code](#)

Data collection No software was used for data collection

Data analysis The codes used for the data analysis are available at github.com/sandrejev/drugs_bioaccumulation. Software used (application detailed in the manuscript): Topspin 3.5 (Bruker), Xcalibur Quan Browser software (Thermo Scientific), R statistical environment (V 3.5 onwards), MaxQuant (version 1.5.3.28), preprocessCore library, limma package in R, IsobarQuant and Mascot 2.4 (Matrix Science), EC2KEGG tool, Blast2GO tool, TPP package for R, XCMS R package, MassHunter Qualitative Analysis Software (Agilent, version 10.0), Mass Profiler Professional (Agilent, version 15.1), OrgMassSpecR-v0.5-3.

For manuscripts utilizing custom algorithms or software that are central to the research but not yet described in published literature, software must be made available to editors and reviewers. We strongly encourage code deposition in a community repository (e.g. GitHub). See the Nature Research [guidelines for submitting code & software](#) for further information.

Data

Policy information about [availability of data](#)

All manuscripts must include a [data availability statement](#). This statement should provide the following information, where applicable:

- Accession codes, unique identifiers, or web links for publicly available datasets
- A list of figures that have associated raw data
- A description of any restrictions on data availability

All data generated during this study are included in this published article (and its supplementary information files). Suppl. Table 18 provides overview of the different methods and data associated with all figures. UPLC and mass-spectrometry data are deposited at the Metabolights repository under the accession codes MTBLS1264 (ebi.ac.uk/metabolights/MTBLS1264), MTBLS1757 (ebi.ac.uk/metabolights/MTBLS1757), MTBLS1627 (ebi.ac.uk/metabolights/MTBLS1627), MTBLS1319 (ebi.ac.uk/metabolights/MTBLS1319), MTBLS1791 (ebi.ac.uk/metabolights/MTBLS1791), MTBLS1792 (ebi.ac.uk/metabolights/MTBLS1792), and MTBLS2885

(ebi.ac.uk/metabolights/MTBLS2885). The mass spectrometry proteomics data have been deposited to the ProteomeXchange Consortium with the dataset identifiers PXD016062 (ebi.ac.uk/pride/archive/projects/PXD016062) and PXD016064 (ebi.ac.uk/pride/archive/projects/PXD016064).

Field-specific reporting

Please select the one below that is the best fit for your research. If you are not sure, read the appropriate sections before making your selection.

Life sciences Behavioural & social sciences Ecological, evolutionary & environmental sciences

For a reference copy of the document with all sections, see nature.com/documents/nr-reporting-summary-flat.pdf

Life sciences study design

All studies must disclose on these points even when the disclosure is negative.

Sample size	No prior assumptions were made regarding effect sizes. Sample sizes were chosen based on prior experience and previous literature on similar experiments. All relevant and possible data points were used for statistical comparisons when applicable.
Data exclusions	No data were excluded from the analysis.
Replication	Biological experiments were performed independently of each other, including media preparation. Screening experiments were performed in independent batches. The main finding (drug bio-accumulation) was verified using different analytical methods (UPLC, MS, NMR), by following the molecular effects using proteomics & metabolomics, and through behavioral assays in <i>C. elegans</i> .
Randomization	Randomization was not relevant as the study was observational and microbiological assays could be performed in desired replicates.
Blinding	Blinding was not relevant as the study did not include analysis of the effects of specific interventions/perturbations and the overall aim was discovery oriented.

Reporting for specific materials, systems and methods

We require information from authors about some types of materials, experimental systems and methods used in many studies. Here, indicate whether each material, system or method listed is relevant to your study. If you are not sure if a list item applies to your research, read the appropriate section before selecting a response.

Materials & experimental systems

- | | |
|-------------------------------------|---|
| n/a | Involved in the study |
| <input checked="" type="checkbox"/> | <input type="checkbox"/> Antibodies |
| <input checked="" type="checkbox"/> | <input type="checkbox"/> Eukaryotic cell lines |
| <input checked="" type="checkbox"/> | <input type="checkbox"/> Palaeontology and archaeology |
| <input type="checkbox"/> | <input checked="" type="checkbox"/> Animals and other organisms |
| <input checked="" type="checkbox"/> | <input type="checkbox"/> Human research participants |
| <input checked="" type="checkbox"/> | <input type="checkbox"/> Clinical data |
| <input checked="" type="checkbox"/> | <input type="checkbox"/> Dual use research of concern |

Methods

- | | |
|-------------------------------------|---|
| n/a | Involved in the study |
| <input checked="" type="checkbox"/> | <input type="checkbox"/> ChIP-seq |
| <input checked="" type="checkbox"/> | <input type="checkbox"/> Flow cytometry |
| <input checked="" type="checkbox"/> | <input type="checkbox"/> MRI-based neuroimaging |

Animals and other organisms

Policy information about [studies involving animals; ARRIVE guidelines](#) recommended for reporting animal research

Laboratory animals	C. elegans (wildtype, strain N2) were used; sex: Hermaphrodite; age: L4 larvae.
Wild animals	No wild animals were used in the study.
Field-collected samples	No field collected samples were used in the study.
Ethics oversight	The study did not require ethical approval

Note that full information on the approval of the study protocol must also be provided in the manuscript.